



**HAL**  
open science

## Quinazoline-based VEGFR-2 inhibitors as potential anti-angiogenic agents: A contemporary perspective of SAR and molecular docking studies

Mahfam Moradi, Alireza Mousavi, Zahra Emamgholipour, Johanna Giovannini, Setareh Moghimi, Fariba Peytam, Amin Honarmand, Stéphane Bach, Alireza Foroumadi

### ► To cite this version:

Mahfam Moradi, Alireza Mousavi, Zahra Emamgholipour, Johanna Giovannini, Setareh Moghimi, et al.. Quinazoline-based VEGFR-2 inhibitors as potential anti-angiogenic agents: A contemporary perspective of SAR and molecular docking studies. *European Journal of Medicinal Chemistry*, 2023, 259, pp.115626. 10.1016/j.ejmech.2023.115626 . hal-04165313

**HAL Id: hal-04165313**

<https://hal.sorbonne-universite.fr/hal-04165313v1>

Submitted on 18 Jul 2023

**HAL** is a multi-disciplinary open access archive for the deposit and dissemination of scientific research documents, whether they are published or not. The documents may come from teaching and research institutions in France or abroad, or from public or private research centers.

L'archive ouverte pluridisciplinaire **HAL**, est destinée au dépôt et à la diffusion de documents scientifiques de niveau recherche, publiés ou non, émanant des établissements d'enseignement et de recherche français ou étrangers, des laboratoires publics ou privés.

# Quinazoline-based VEGFR-2 inhibitors as potential anti-angiogenic agents: A contemporary perspective of SAR and molecular docking studies

Mahfam Moradi <sup>a</sup> †, Alireza Mousavi <sup>a</sup> †, Zahra Emamgholipour <sup>a</sup>, Johanna Giovannini <sup>b</sup>, Setareh Moghimi <sup>c</sup>, Fariba Peytam <sup>c</sup>, Amin Honarmand <sup>d</sup>, Stéphane Bach <sup>b,e,f,\*</sup>, Alireza Foroumadi <sup>a,c,d,\*</sup>

<sup>a</sup> Department of Medicinal Chemistry, Faculty of Pharmacy, Tehran University of Medical Sciences, Tehran, Iran

<sup>b</sup> Sorbonne Université, CNRS, UMR8227, Integrative Biology of Marine Models Laboratory (LBI2M), Station Biologique de Roscoff, 29680 Roscoff, France.

<sup>c</sup> Drug Design and Development Research Center, The Institute of Pharmaceutical Sciences (TIPS), Tehran University of Medical Sciences, Tehran, Iran

<sup>d</sup> Neuroscience Research Center, Institute of Neuropharmacology, Kerman University of Medical Sciences, Kerman, Iran

<sup>e</sup> Sorbonne Université, CNRS, FR2424, Plateforme de criblage KISSf (Kinase Inhibitor Specialized Screening facility), Station Biologique de Roscoff, 29680 Roscoff, France.

<sup>f</sup> Centre of Excellence for Pharmaceutical Sciences, North-West University, Private Bag X6001, Potchefstroom 2520, South Africa.

† These authors contributed equally to this work.

## Corresponding authors:

Dr. Stéphane Bach: [stephanebachcnrs@gmail.com](mailto:stephanebachcnrs@gmail.com)

Prof. Alireza Foroumadi: [aforoumadi@yahoo.com](mailto:aforoumadi@yahoo.com)

## **Abstract**

Angiogenesis, the formation of new blood vessels from the existing vasculature, is pivotal in the migration, growth, and differentiation of endothelial cells in normal physiological conditions. In various types of tumour microenvironments, dysregulated angiogenesis plays a crucial role in supplying oxygen and nutrients to cancerous cells, leading to tumour size growth. VEGFR-2 tyrosine kinase has been extensively studied as a critical regulator of angiogenesis; thus, inhibition of VEGFR-2 has been widely used for cancer treatments in recent years. Quinazoline nucleus is a privileged and versatile scaffold with a broad range of pharmacological activity, especially in the field of tyrosine kinase inhibitors with more than twenty small molecule inhibitors approved by the US Food and Drug Administration in the last two decades. As of now, the U.S. FDA has approved eleven small chemical inhibitors of VEGFR-2 for various types of malignancies, with a prime example being vandetanib, a quinazoline derivative, which is a multi targeted kinase inhibitor used for the treatment of late-stage medullary thyroid cancer. Despite of prosperous discovery and development of VEGFR-2 down regulator drugs, there still exists limitations in clinical efficacy, adverse effects, a high rate of clinical discontinuation and drug resistance. Therefore, there is an urgent need for the design and synthesis of more selective and effective inhibitors to tackle these challenges. Through the gathering of this review, we have strived to broaden the extent of our view over the entire scope of quinazoline-based VEGFR-2 inhibitors. Herein, we give an overview of the importance and advancement status of reported structures, highlighting the SAR, biological evaluations and their binding modes.

## Contents

Keywords .....	3
Abbreviations .....	4
Symbols.....	6
Introduction.....	7
Angiogenesis.....	7
Vascular Endothelial Growth Factor Receptor .....	7
Structure of VEGFR-2 .....	8
Small molecule VEGFR-2 inhibitors.....	9
Quinazolines .....	9
Clinical development of quinazoline based VEGFR-2 inhibitors .....	10
Binding site of VEGFR-2 .....	11
Classification of VEGFR-2 inhibitors according to binding mode .....	13
Development of quinazoline based VEGFR-2 inhibitors .....	14
Functionalization of quinazoline with aryl rings .....	14
Functionalization of Quinazoline Core with Hydrogen Bond Donor/Acceptor Groups .....	24
Equipment of HB donor/acceptor groups at C-4 position .....	24
Equipment of HB donor/acceptor groups at C-4 position linked by an aliphatic chain .....	47
Equipment of HB donor/acceptor groups at C-5 position .....	49
Equipment of HB donor/acceptor groups at C-7 position .....	51
Equipment of HB donor/acceptor groups at C-2 or N-3 positions .....	53
Irreversible inhibitors.....	62
Conclusion .....	64
Declaration of competing interest.....	65
Acknowledgments.....	65
References.....	65

## Keywords

Quinazoline, VEGFR-2, Angiogenesis, Kinase, TKI, SAR

## Abbreviations

3D QSAR	Three-dimensional quantitative structure-activity relationship
Abl	Abelson
Akt	Protein kinase B
Asn	Asparagine
Asp	Aspartic acid
ATP	Adenosine triphosphate
Bax	Bcl-2-associated X
Bcl-2	B-cell lymphoma-2
bFGF	Basic fibroblast growth factor
B-Raf	B-rapidly accelerated fibrosarcoma
BTK	Bruton's tyrosine kinase
CA-4	Combretastatin A-4
CAM	Chorioallantoic membrane
CCK8	Cell Counting Kit 8
c-Kit	Cluster of differentiation 117
Cl	Clearance
c-Met	Hepatocyte growth factor receptor
CoMFA	Comparative Molecular Field Analysis
CoMSIA	Comparative molecular similarity indices analysis
CSF-1R	Colony stimulating factor 1 receptor
Cys	Cysteine
DFG	Dynamic form generator
DMPK	Drug metabolism and pharmacokinetics
EGF	Epidermal growth factor
EGFR	Epidermal growth factor receptor
EphB4	Ephrin type-B receptor 4
FAK	Focal adhesion kinase
FDA	Food and Drug Administration
FGF	Fibroblast growth factor
FGFR-1	Fibroblast growth factor receptor-1
FGFR-4	Fibroblast growth factor receptor-4
Flk-1	Fetal liver kinase-1
FLT1	Fms-related receptor tyrosine kinase 1
FLT-3	Fms like tyrosine kinase-3
FLT4	Fms-related receptor tyrosine kinase-4

GI	Growth inhibition
GIST	Gastrointestinal stromal tumour
Glu	Glutamic acid
Gly	Glycine
GSH	Glutathione
HB	Hydrogen bond
HEK293	Human embryonic kidney 293 cell
HER-2	Human epidermal growth factor receptor 2
HGF	Hepatocyte growth factor
HOMO	Highest occupied molecular orbital
HTRF	Homogeneous Time Resolved Fluorescence
HUVEC	Human umbilical vein endothelial cells
Ile	Isoleucine
IPF	Idiopathic pulmonary fibrosis
KDR	Kinase Insert Domain Receptor
LCK	Lymphocyte-specific protein tyrosine kinase
Leu	Leucine
LUMO	Lowest Unoccupied Molecular Orbital
Lys	Lysine
mCRC	Metastatic colorectal cancer
MDR1	Multidrug resistance 1
MMP	Mitochondrial membrane potential
MTC	Medullary thyroid cancer
NCI	National Cancer Institute
NSCLC	Non-Small Cell Lung Cancer
PDGF	Platelet-derived growth factor
PDGFR	Platelet-derived growth factor receptor
PDGFR- $\beta$	Platelet derived growth factor receptor beta
Pgp	permeability glycoprotein
Phe	Phenylalanine
PI	Propidium iodide
PI3K	Phosphoinositide 3-kinase
PK	Pharmacokinetics
RCC	Renal cell carcinoma
RET	Rearranged during transfection
RET	Rearranged during transfection

ROS	Reactive oxygen species
RPTEC	Renal proximal tubule epithelial cells
SAR	Structure-activity relationship
Sck	Serum creatine kinase
Src	Sarcoma
TGI	Tumor growth inhibition
Thr	Threonine
Tie-2	Angiopoietin-1 receptor
TSP	Thrombospondin
Tyr	Tyrosine
Val	Valine
VEGF	Vascular endothelial growth factor
VEGF-A	Vascular endothelial growth factor A
VEGF-B	Vascular endothelial growth factor B
VEGF-C	Vascular endothelial growth factor C
VEGF-D	Vascular endothelial growth factor D
VEGF-E	Vascular endothelial growth factor E
VEGF-F	Vascular endothelial growth factor F
VEGFR	Vascular endothelial growth factor receptor
VEGFR-1	Vascular epidermal growth factor receptor-1
VEGFR-2	Vascular epidermal growth factor receptor-2
VEGFR-3	Vascular epidermal growth factor receptor-3

## **Symbols**

F	Bioavailability
GI <sub>50</sub>	Half maximal growth inhibition
IC <sub>50</sub>	Half maximal inhibitory concentration
IV <sub>t1/2</sub>	Intravenous half-life
LC <sub>50</sub>	Half maximal lethal concentration
Log D	Log distribution coefficient
V <sub>dss</sub>	Steady-state volume of distribution

## **Introduction**

### **Angiogenesis**

Angiogenesis is the process of new blood vessel growth from pre-existing microvascular structures (1). This process begins with endothelial cell activation, vascular basement membrane dilatation, and permeability of the interstitial matrix increase (2). This biological signaling plays a vital role in endothelial cell proliferation, survival, and migration (3). Normal physiological angiogenesis is strictly regulated by a variety of stimulating and suppressing factors. In particular, proangiogenic factors including growth factors such as VEGF, FGF, PDGF, HGF and EGF, adhesion factors, proteinases, extracellular matrix proteins, transcription molecules and signaling factors, are in balance with antiangiogenic factors including TSP, angiostatin, and endostatin (4, 5). Under pathological conditions, there is a rise in the factors promoting angiogenesis that can consequently effect tumour formation and chronic conditions such as retinopathies, arthritis, endometriosis and atherosclerosis (6). It is notable that the angiogenesis role in tumour microenvironment was first observed by Folkman in 1971 who described tumours as "hot and bloody" (7).

### **Vascular Endothelial Growth Factor Receptor**

Preceding the tumour growth beyond a certain size, hypoxic conditions initiate spontaneous secretion of angiogenic stimulators, which is a fundamental step for the transition of a benign tumour to a malignant state (8, 9). Vascular endothelial growth factor (VEGF) has been demonstrated to be a significant angiogenesis contributor, increasing the number of capillaries and upregulating the signaling cascade relating to angiogenesis (10). Many types of cancer, especially colorectal and kidney carcinomas, express elevated levels of VEGF (11, 12). Therefore, VEGF subtypes and their associated tyrosine kinase receptors (VEGFRs) have been considered attractive targets for the inhibition tumour growth (13). The family of VEGF consists of VEGF-A, VEGF-B, VEGF-C, VEGF-D, VEGF-E, VEGF-F and placental growth factor (PlGF) (14). These proteins show different affinities for VEGFR isoforms (10). VEGFR exists as three subtypes, VEGFR-1 (FLT1), VEGFR-2 (KDR in humans or Flk-1 in mice), and VEGFR-3 (FLT4) (15, 16). Among these three VEGFRs, VEGFR-2 has a pivotal impact on advancing angiogenesis and neovascularization in pathological and physiological conditions and is



expressed predominantly on vascular endothelial cells, causing it to be the most significant target in anti-angiogenic therapy (13).

The binding of VEGF ligands to VEGFR-2 causes dimerization followed by autophosphorylation of this receptor, regularly occurring in Tyr1175 and Tyr1214 residues (17). Multiple downstream pathways are activated by autophosphorylated VEGFR-2, such as PI3K, Sck, FAK, Src, and Akt, which are typically hyperactivated in several tumour types (18). Tugues et al. has shown that in endothelial cells, the interaction of VEGFR2 with CD63, a member of the transmembrane-4 glycoprotein superfamily (tetraspanins), is required for VEGFR-2 phosphorylation, efficient internalization of VEGFR-2 and subsequent downstream signaling (19).

### Structure of VEGFR-2

VEGFR-2 extracellular structure is composed of an extracellular ligand-binding domain, with a short N-terminal signal sequence followed by seven immunoglobulin (Ig)-like segments, connected by a transmembrane domain to the intracellular part, which consists of a juxtamembrane domain, a split tyrosine kinase domain, and a larger C-terminus tail (Fig. 1) (20).

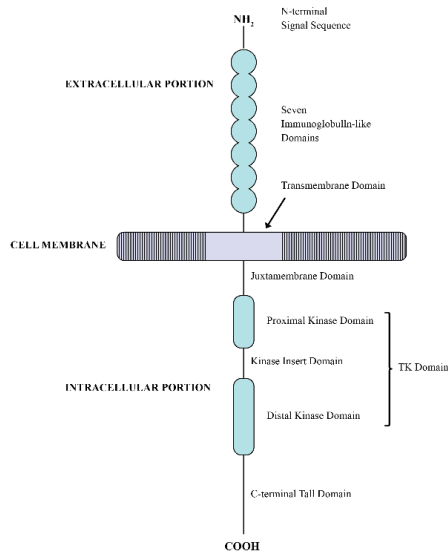


**Figure 1.** Schematic view of VEGFR functional domains.

## Small molecule VEGFR-2 inhibitors

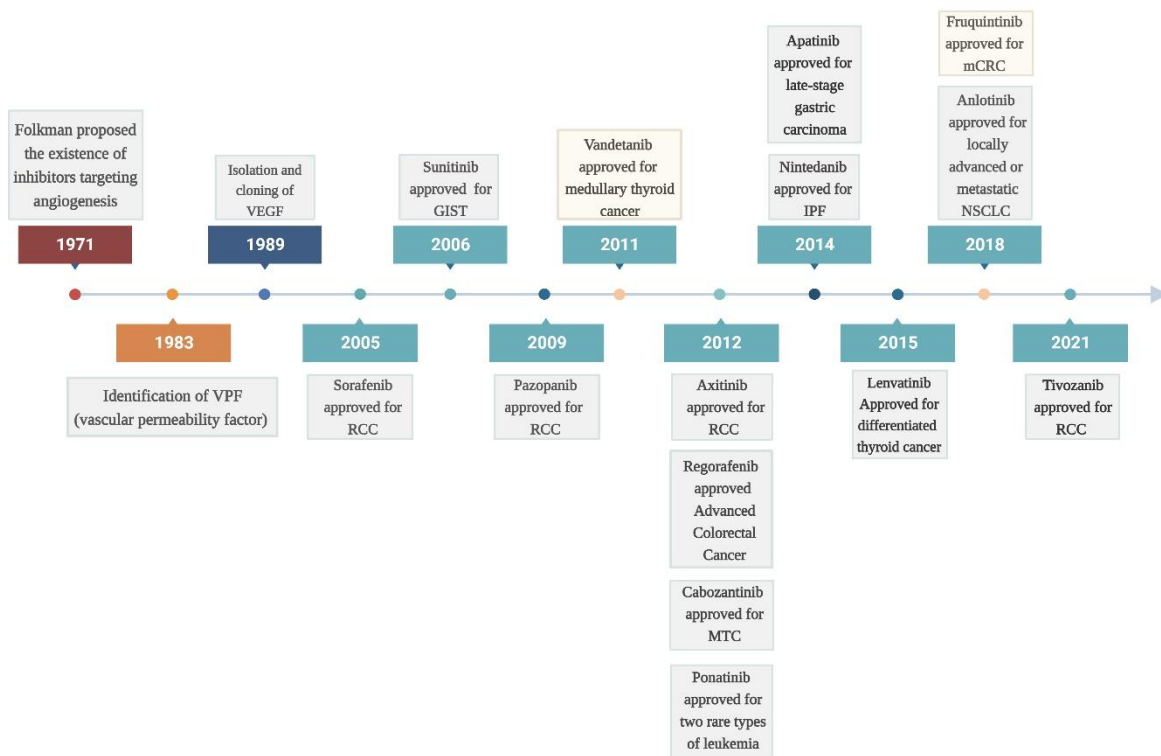


**Figure 2.** Key events in VEGFR inhibitor development.

In recent years, several small molecules were approved by FDA as inhibitors of VEGFR-2 for various types of cancers, namely sunitinib, sorafenib, vandetanib, pazopanib, axitinib, cabozantinib, regorafenib, nintedanib, ponatinib, and lenvatinib. The most recent approval was in 2021 for tivozanib to treat advanced renal cell carcinoma. (21)

## Quinazolines

Quinazoline is a nitrogen-containing aromatic bicyclic heterocycle consisting of two fused six-membered rings, benzene and pyrimidine (22). Quinazoline-based compounds display a wide range of biological activities, such as analgesic(23), antioxidant(24), anti-inflammatory(25), anti-bacterial(26), antiviral(27), anti-diabetic(28), anti-malarial(29), anti-hypertensive(30) and anti-cancer activities(31, 32). Exploration of quinazoline and its derivatives demonstrated their great potential as promising kinase inhibitors, which are one of the most identified targets in anti-cancer drug discovery, and were found in approved drugs targeting EGFR, VEGFR-2, HER-2 and PI3K kinases (33, 34).

## Clinical development of quinazoline based VEGFR-2 inhibitors

In recent years, several quinazoline-based agents as VEGFR-2 inhibitors have been investigated in clinical trials as a single treatment or in combination with other drugs(35), which are listed below.

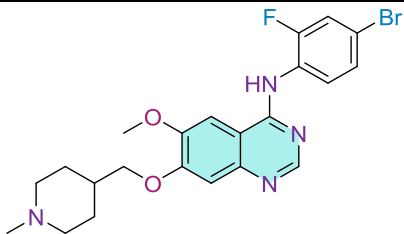
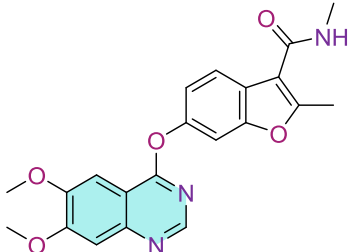
Vandetanib (ZD6474), trade name Caprelsa, developed by AstraZeneca, is a quinazoline-based drug that inhibits VEGFR-2, EGFR, RET, Brk, Tie2, EphRs and Src family of kinases. FDA approved vandetanib in April 2011 as the first drug to treat late-stage (metastatic) medullary thyroid cancer among adult patients who are ineligible for surgery (36).

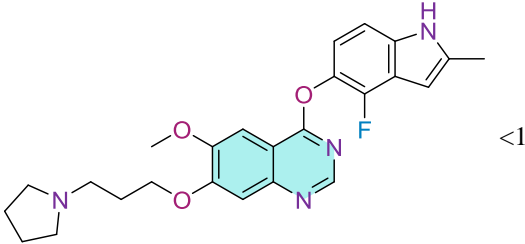
Fruquintinib (HMPL-013), trade name Elunate, is a potent and highly selective VEGFR-1, -2 and -3, received its first global approval in China in 2018 for the treatment of metastatic colorectal cancer in patients with failure in at least two previous systemic anti-neoplastic therapies(37).

Cediranib (AZD2171) is a highly potent VEGFR-2 inhibitor developed by AstraZeneca. It has completed several clinical trials since 2007 and is currently being investigated in phase III for ovarian cancer treatment in combination with olaparib (38).

**Table 1**

quinazoline based VEGFR-2 drugs

Name	Structure	VEGFR-2 Potency (IC <sub>50</sub> nM)	Targets	Approval Date	Indication
Vandetanib		30	VEGFR-2, EGFR, RET	2011	late-stage medullary thyroid cancer
Fruquintinib		35	VEGFR-1, -2, -3	2018 China	metastatic colorectal cancer

Cediranib		<1	VEGFR- 1, -2, -3, c-Kit PDGFR- $\alpha$ , $\beta$	phase III	ovarian cancer
-----------	-----------------------------------------------------------------------------------	----	---------------------------------------------------------------	-----------	-------------------

### Binding site of VEGFR-2

Binding site analysis of VEGFR-2 (Fig. 3) revealed that it can be divided into four sections, in particular, a hinge region, the DFG motif and hydrophobic pockets I and II. The hinge region consists of two essential residues, namely Cys919 and Glu917, that create crucial hydrogen bonds necessary to maintain the inhibitory activity. This hydrogen bond rich domain is favorably occupied by hydrogen bond donor and acceptor groups linked in particular to Asp1046 and Glu885 residues. The hydrophobic pocket I is surrounded by three amino acids, Gly992, Leu840, and Phe918, that can accommodate monocyclic or bicyclic ring structures, and the hydrophobic pocket II is surrounded by four amino acid residues, namely, Ile892, Ile1044, Leu889, and Val898. (39)

The DGF motif is a conserved pocket generally consisting of three amino acids, which in VEGFR-2 is made up of Asp1046, Phe1047, and Gly1048 residues. Based on the arrangement of this motif in the kinase domain, there are active (DFG-in, Fig. 4a) and inactive states (DFG-out, Fig. 4b). The difference between these states can be assigned to the orientation of the side chain of Phe1047. In the DFG-in conformation, Phe1047 residue inserts into the allosteric site. In contrast, in the DFG-out conformation, Phe1047 residue turns outwards to the phosphate/sugar region, resulting in an empty allosteric area and a slim linker site (40).

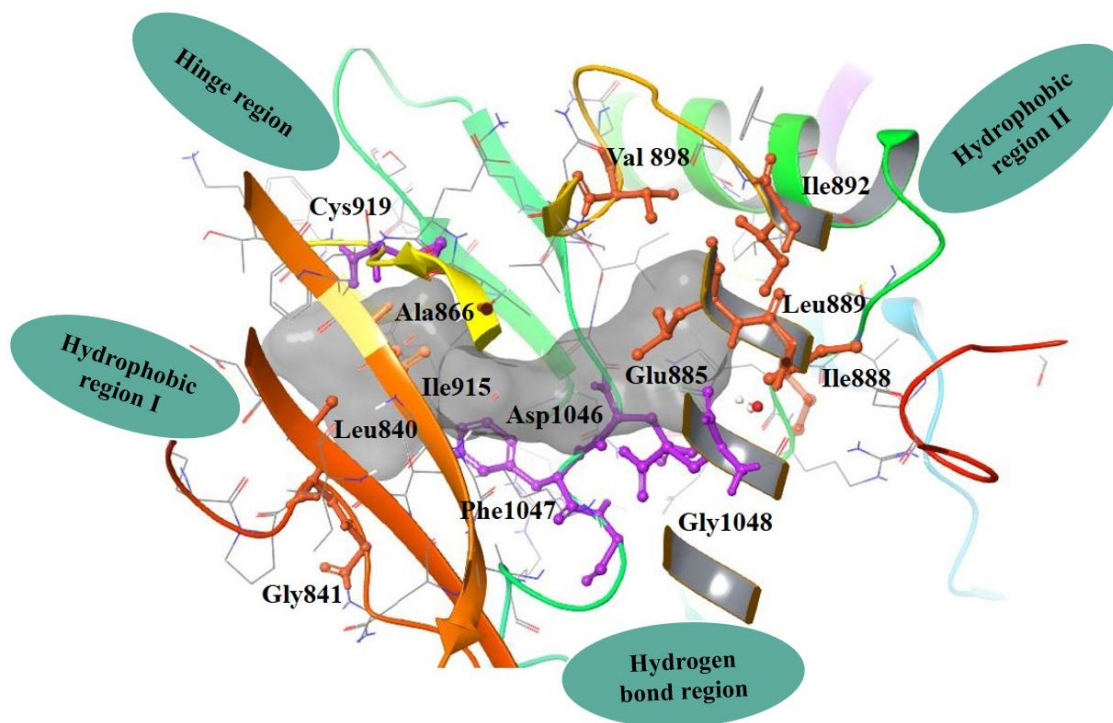


**Figure 3.** Binding site analysis of VEGFR-2

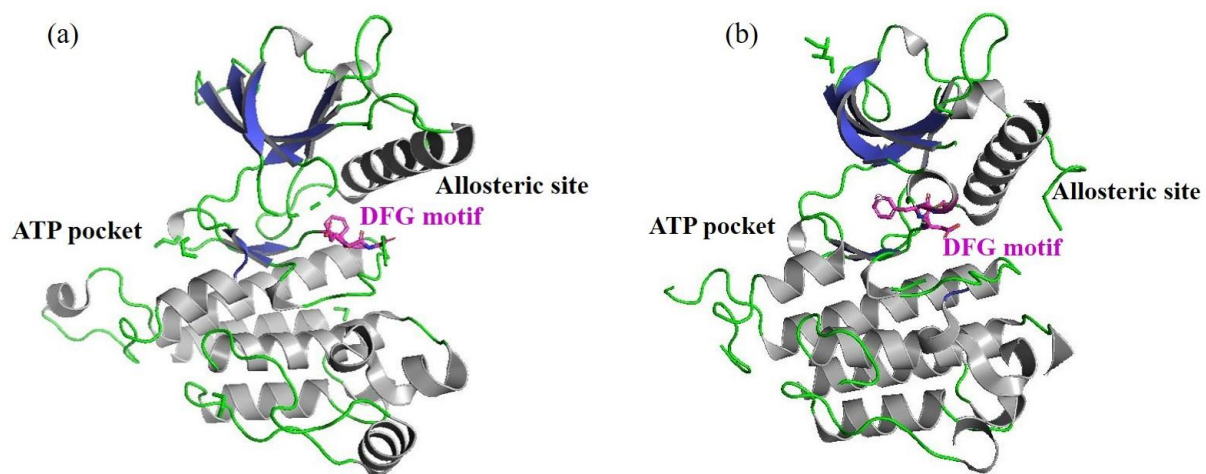


**Figure 4.** Structure of VEGFR2 in the DFG-in (a) and DFG-out states (b).

### **Classification of VEGFR-2 inhibitors according to binding mode**

Identifying key structural elements that interact with the highly conserved active site of the kinase domain, which is responsible for binding ATP, is an important aspect of designing VEGFR-2 inhibitors. Extensive studies on the pharmacophoric features of these inhibitors have revealed that: (i) firstly, a heteroaromatic moiety plays a crucial role in interacting with the hinge region (prominent examples of these moieties include indolinone(41), quinoline(42), pyridine(43), pyrimidine(44), and quinazoline), (ii) secondly, a spacer group that occupies the gatekeeper region which can accommodate monocyclic or bicyclic rings, (iii) thirdly, the placement of hydrogen bond acceptor/donor groups that bind to the DFG motif which plays pivotal role in the regulation of kinase activity and conformational dynamics, and (iv) lastly, the incorporation of a terminal hydrophobic moiety for establishing favorable hydrophobic interactions with the allosteric hydrophobic pocket within the ATP binding site.

According to the canonical classification of VEGFR-2 inhibitors (45), there are two types of interaction between the ligand and the active site of the kinase.

#### **Type I inhibitors**

Type I inhibitors bind to active conformation of the VEGFR-2 by occupying hydrophobic pocket I in addition with having multiple hydrogen bonds with hinge and DFG regions. In type I inhibition, the binding mode has an overlap with the adenine ring of the ATP, making them ATP competitive inhibitors. Vandetanib, sunitinib, cediranib and semaxinib are examples of this type of inhibitors. (46)

#### **Type II inhibitors**

The inactive form of VEGFR-2 has DFG-out conformation resulting in appearance an extra hydrophobic binding pocket (hydrophobic pocket II). In addition to essential interactions with other sites, type II inhibitors interact with this region, therefore they can inhibit the enzyme without competing with ATP. Examples of type II inhibitors are sorafenib, foretinib, regorafenib, and tivozanib. (46)

The aim of this review is to provide an overview of the latest findings on the discovery and development of compounds containing quinazoline core as small molecule VEGFR-2 inhibitors.

Further strategies for designing and developing selective quinazoline-based inhibitors will be discussed in detail.

### Development of quinazoline based VEGFR-2 inhibitors

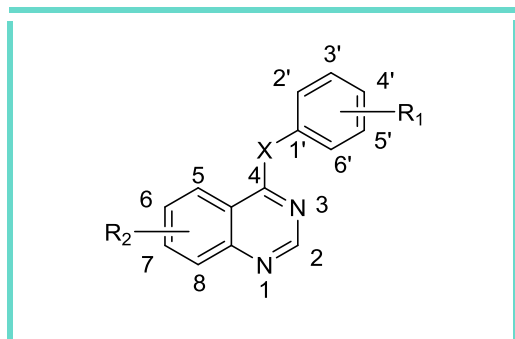


**Figure 5.** General quinazoline derivatives numbering system

### Functionalization of quinazoline with aryl rings

In general, the C-4 position of the quinazoline ring is a critical position for modifications in literature, examined with various substituent placements, mostly with different aryl rings. These C-4 aromatic rings are linked to the quinazoline core with diverse linker atoms, which can contain different substituents varying in size and polarity. This region usually locates in the hydrophobic pocket I of the VEGFR-2 active site, constituting type I inhibitors. In most cases, manipulation of the C-6 and C-7 positions on the quinazoline core is related to enhancing the pharmacokinetic profile.

Screening of Zeneca's library of compounds led to the introduction of a series of 4-anilinoquinazoline derivatives as selective micromolar VEGFR-2 inhibitors compared to VEGFR-1 and FGFR-1 kinases (47). The introduction of small substituents such as fluorine at the C-2' position, hydroxyl group at C-3' or C-5', and small lipophilic substituents such as halogens or methyl at the C-4' position increased the inhibitory activity. Investigation of the C-6 position of the quinazoline ring indicated that the methoxy group is the most preferred substituent; however, the C-7 position can tolerate a large range of neutral, basic and heteroaromatic side chains. The most potent compound was **1** (Fig. 6), which inhibited VEGFR-2 with an  $IC_{50}$  value less than 2 nM. Examination of **1** in cellular proliferation assay revealed that it could inhibit VEGF-driven HUVEC (V-HUVEC) with an  $IC_{50}$  value of 4 nM in comparison to 800 nM against fibroblast growth factor driven HUVEC (F-HUVEC). However, it showed low

plasma level concentration in mice. Therefore, further modifications resulted in compound **2** (ZD4190) (Fig. 6), which had plasma levels of 13  $\mu\text{M}$  for as long as 24h (enzymatic and cellular properties of **2** are shown in **Table 2**). In an *in vivo* study, **2** showed 75% growth inhibition in Calu-6 tumour xenografts by oral administration of 100 mg/kg/day for 21 days.

Following the previous study, considering the PK properties of compound **2**, Hennequin *et al.* introduced a novel series of 4-anilinoquinazolines in an attempt to enhance its anticancer activity profile (48). Even though compound **2** had optimal antitumour activities in *in vitro* and *in vivo* (**Table 2**), it had some drawbacks, such as poor solubility and a low percentage of oral bioavailability in dog. Therefore, various substituents were examined at the C-7 position of the quinazoline core; among those, nitrogen-containing basic residues revealed superior solubility at physiological pH of 7.4. Considering all the parameters, compound **3** (ZD6474, vandetanib) was introduced, with up to 400-fold improvement in aqueous solubility and up to a 10-fold increase in *in vivo* assessments for oral bioavailability in dog (as shown in detail in **Table 3**). Enzymatic and cellular assessment of compound **3** compared to **2** showed a more selective VEGFR-2 and V-HUVEC inhibition profile (**Table 2**). *In vivo* assay of **3** (Fig. 6) revealed a noteworthy, dose-dependent antitumour activity by inhibiting the growth of Calu-6 lung carcinoma xenografts by 79%, with once-daily oral administration of 100 mg/kg for 21 days.

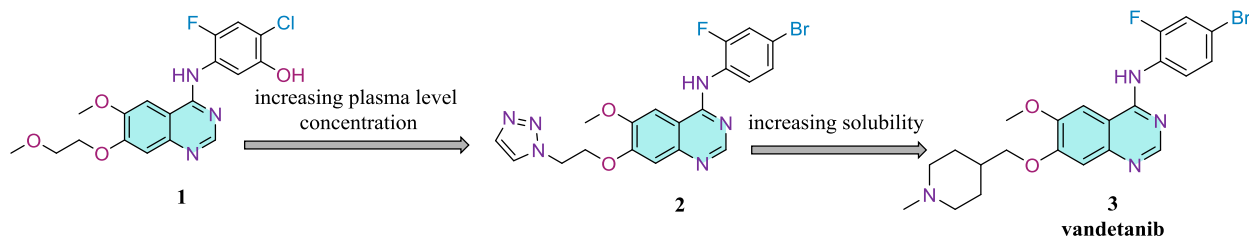


**Figure 6.** Structural representation of **1-3**.

**Table 2**

Results of biological evaluation of compound **2** and **3** (data extracted from (48)).

Compounds	Inhibiton Level (IC <sub>50</sub> , $\mu\text{M}$ )				Effect on Cell Viability (EC <sub>50</sub> , $\mu\text{M}$ )		
	VEGFR-2	VEGFR-1	EGFR	PDGFR- $\beta$	V-HUVEC	F-HUVEC	Unstimulated HUVEC
<b>2</b>	0.03	0.7	0.4	3.4	0.05	0.05	>10



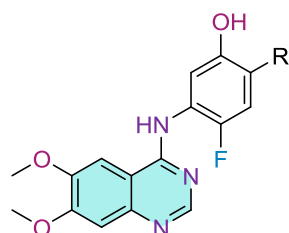
<b>3</b>	0.04	1.6	0.5	1.1	0.06	-	>3
----------	------	-----	-----	-----	------	---	----

**Table 3**

Results of PK evaluation of compound **2** and **3** (data extracted from (48)).

Compounds	IV $t_{1/2}$ (h)	F (%)
<b>2</b>	1.1	<5
<b>3</b>	8.3	>50

Newton and coworkers reported a series of 4-anilino-6,7-dimethoxy quinazoline derivatives in an approach to explore the selectivity of these compounds against VEGFR-2 and RET based on the similarity of their ATP-binding site (49). It became apparent that placing a hydroxy group at C-3' position considerably enhanced the VEGFR-2 affinity; therefore, this substituent remained still in most of the compounds. The inclusion of any substituents bigger than a Fluorine atom at C-2' dramatically reduced the VEGFR-2 inhibition. Overall, the insertion of halogens at C-4', C-5', and C-6' positions increased the enzymatic activity. In addition, the linker atom between the quinazoline core and aniline moiety showed VEGFR-2 selectivity in this decreasing order: O > S > NMe. To investigate the cellular activity, modified BaF3 (murine interleukin-3 dependent pro-B cells) cell line were used to express activated recombinant RET and VEGFR-2 kinases. In general, VEGFR-2 inhibitory activity is more correlated with its cellular and enzymatic activities than RET kinase. Compounds **4** and **5** (Fig. 7) were the most promising compounds regarding affinity to VEGFR-2 with  $IC_{50}$  values of 2.3 and 9.5 nM, respectively, also activity in cell assay with  $IC_{50}$  values of 9.5 and 66 nM, respectively. Further biological profiling of compound **4** revealed insufficient intrinsic clearance in human hepatocytes ( $Cl_{int}$  91.9  $\mu$ L/min/ $10^6$  cells).



**4:** R= CH<sub>3</sub>

**5:** R=F

**Figure 7.** Structural representation of **4** and **5**.

Based on canertinib and vandetanib, Bang *et al.* designed a series of hybrid compounds containing acryl amide at C-6 position and 4-bromo-2-fluoroaniline at C-4 position of quinazoline core as dual EGFR and VEGFR-2 inhibitors (50). According to the SAR study, they examined a different number of carbon atoms at the C-7 position side chain, revealing that compounds with short carbon chains were more active on VEGFR-2 than those with longer aliphatic chains. Afterwards, by fixing the carbon chain at n=1, various derivatives containing alkyl or hetero alkyl groups attached to amido moiety were examined. Among them, compound **6** (Fig. 8) displayed the best enzymatic activity ( $IC_{50}$  =2 nM against EGFR and  $IC_{50}$  = 103 nM against VEGFR-2). Performing Matrigel Plug assay and cell-based inhibitory activity against VEGF-induced HUVEC revealed that **6** could inhibit angiogenesis in both *in vitro* and *in vivo* experiments. Moreover, **6** did not show inhibitory effect on Hs27 (human foreskin fibroblast cells) up to 1  $\mu$ M.

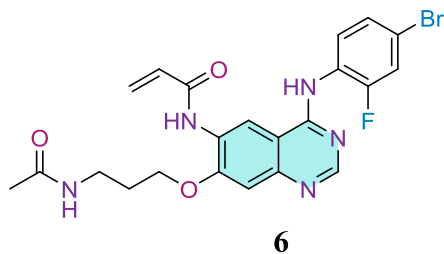


**Figure 8.** Structural representation of **6**.

Pathological hypoxia is a fundamental incompatibility of solid tumours and healthy tissues; hence modifications like the insertion of moieties with high affinity to hypoxic regions presumably result in compounds with less adverse effects and high specificity for hypoxic-adapted malignant tissues (51, 52). Wei and colleagues developed a hypoxia-activated vandetanib derivative **7** by introducing a nitroimidazole group in the piperidine side chain. However, toxicity limitations and multiple adverse reactions were observed during the *in vivo* study (53). Consequently, 3-nitro-1,2,4-triazole moiety linked to the 4-anilinoquinazoline core was introduced as hypoxia-targeted compounds with the understanding of better pharmacokinetic property and biosecurity (54). In general, synthesized compounds had better activities against EGFR compared to VEGFR-2. Compounds bearing bulky halogen atoms on aniline moiety had higher the VEGFR-2 inhibition. Under  $CoCl_2$ -induced hypoxia, all compounds showed better

antiproliferative activity compared with normoxic conditions. Compound **8** (Fig. 9), with the best VEGFR-2 inhibition ( $IC_{50} = 36.78$  nM), was the only compound that revealed a higher inhibition percentage in hypoxic conditions and also hypoxic microenvironment combined with irradiation against A549 (adenocarcinomic human alveolar basal epithelial cells) and H446 (human small cell lung cancer cells) cell lines compared those of vandetanib as shown in **Table 4**. Additionally, **8** significantly downregulated VEGF expression better than vandetanib under both normoxic and hypoxic conditions in A549 cells. In the A549 tumour cell xenograft models, oral administration of 10 mg/kg of **8** at day 17 showed a TGI value of 63.93%, similar to that of vandetanib (TGI = 62.06%). However, **8** had a notable safety profile and no significant weight loss was observed upon consumption. Through docking studies, compound **8** was directed towards VEGFR-2 active site with key interactions between N-1 and N-3 of quinazoline nucleus with Cys919 and Thr916 residues, and the Oxygen of the amide moiety with Asn923.

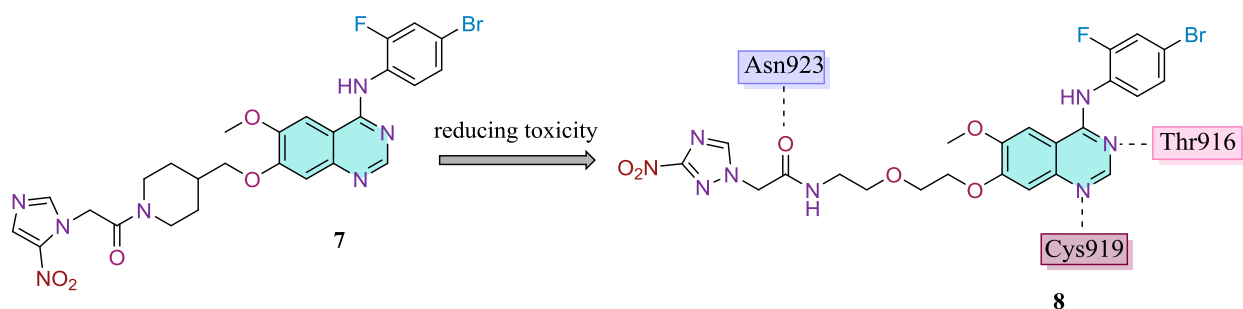


**Figure 9.** Structural representation of **7** and **8**.

**Table 4**

Results of cellular evaluations of compound **8** when tested at 0.5  $\mu$ M (data extracted from (54)).

Compounds	Inhibition Ratios (%)					
	A549 Normoxia	A549 Hypoxia	A549 Hypoxia + IR	H446 Normoxia	H446 Hypoxia	H446 Hypoxia + IR
<b>8</b>	6.75	75.86	86.41	18.95	84.37	88.66
Vandetanib	21.06	67.26	81.44	25.58	77.67	82.02

In an effort to design selective B-Raf inhibitors, Lee *et al.* synthesized a series of 4-anilinoquinazoline linked to a 1,2,3-triazole motif, several of them were also found effective against EGFR and VEGFR-2 (55). Compound **9** (Fig. 10) bearing 2-carbamoyl ethyl side chain was the most potent against B-Raf, B-Raf<sup>V600E</sup>, EGFR and VEGFR-2 ( $IC_{50} = 7$  nM) kinases as

shown in **Table 5**. **9** also exhibited IC<sub>50</sub> values of 6 and 1.3 μM against PC-9 (human non-small cell lung carcinoma) and HCC827 (human lung adenocarcinoma cell line), EGFR-sensitive cells. Further molecular docking of **9** shows a strong bonding with good interaction in the VEGFR-2 binding pocket between N-1 of the quinazoline nucleus and Cys919, and the OH group with Asp1046. Additionally, substituent at the C-6 position formed one hydrogen bond between triazolyl group and Asn923 and two other bonds between the carbamoyl terminus and Phe921 and Asn923 residues.

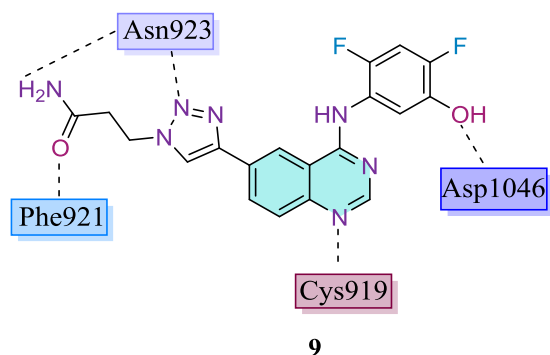


**Figure 10.** Structural representation and binding mode of **9** into VEGFR-2 active site.

**Table 5**

Results of enzymatic evaluations of compound **9** (data extracted from (55)).

Compound	Inhibition Level (IC <sub>50</sub> , μM)				
	B-Raf	B-Raf <sup>V600E</sup>	C-Raf	EGFR	VEGFR-2
<b>9</b>	0.057	0.051	1.0	0.073	0.007

Histone deacetylases (HDAC) are a class of enzymes that remove acetyl groups from an ε-N-acetyl lysine amino acid in histone termini inducing chromatin condensation and transcriptional repression (56). In order to overcome the drug resistance toward single targeted VEGFR-2 inhibitors; Peng *et al.* developed a series of compounds inhibiting both VEGFR-2 and HDAC (57). As mentioned, the C-6 position of the quinazoline core can tolerate different groups; therefore, a hydroxamic acid moiety as a zinc chelating agent in the HDAC active site was bound by a linker of various lengths to the skeleton. The length of the carbon linker did not have significant effects on VEGFR-2 inhibitory activity, although, by increasing the length, the HDAC inhibition increased as well. The halogen substitutions on anilino moiety was a dominating factor for VEGFR-2 inhibition. Compound **10** (Fig. 11), with the optimal 6-carbon chain linker and 2,4-dichloro anilino moiety, had the best VEGFR-2 and HDAC inhibition (IC<sub>50</sub>

values 84 and 2.8 nM, respectively). Furthermore, **10** displayed the best antiproliferative activity against MCF-7 human breast cancer cell line with an  $IC_{50}$  value of 1.2  $\mu$ M accompanied by inhibiting HepG2 (nontumorigenic hepatic cells), A549 and HCT-116 (colon cancer cell line) human cell lines with  $IC_{50}$  values of 2.7, 5.4 and 1.8  $\mu$ M, respectively. Docking simulations revealed that NH of the aniline moiety interacts with Asp1046 residue and the terminal hydroxyl oxygen binds to Cys919 via hydrogen bonds.

Continuing with this study, by Peng et al. revealed that the *para* position of the aniline ring was better compared to the *ortho* position (58). Additionally, the halogen atom at *para* position, increased the inhibitory activity in the following increasing order: F < Cl < Br. Among the synthesized compounds, **11** (Fig. 11) had the best HDAC inhibitory activity ( $IC_{50}$  = 2.2 nM), alongside potent VEGFR-2 inhibition ( $IC_{50}$  = 74 nM). **11** also demonstrated the most potent inhibitory activity against MCF-7 with  $IC_{50}$  of 0.85  $\mu$ M. Docking of compound **11** into ATP binding site of VEGFR-2 revealed a hydrogen bond between carbonyl oxygen and Asn923 along with another interaction with terminal hydroxyl oxygen and Lys868 residue.

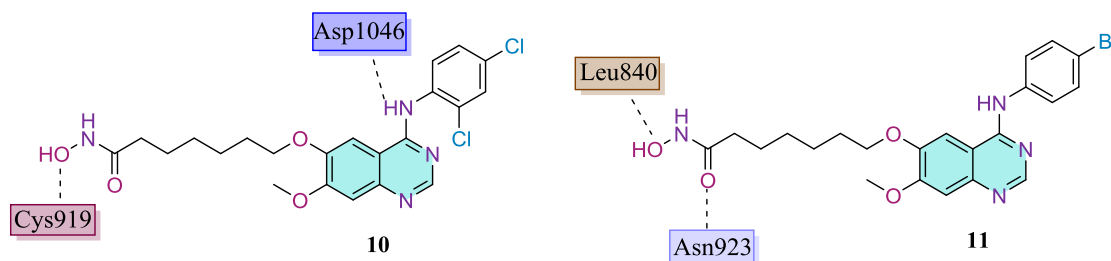


**Figure 11.** Structural representation and binding modes of **10** and **11** into VEGFR-2 active site.

Choudhary *et al.* developed novel derivatives of **12** (verubulin) (Fig. 12), a multi-targeted inhibitor (59). **12** is a quinazoline-based compound that acts as a tubulin polymerization inhibitor and interrupts microtubule formation. However, this compound was used in patients with newly diagnosed Glioblastoma Multiforme (GBM) and discontinued in phase II of clinical trials due to cardiac toxicity (60). Kinase assessment of **12** revealed that it had single-digit nanomolar inhibition against EGFR, VEGFR-2 and PDGFR- $\beta$  ( $IC_{50}$  values 2.8, 8.4 and 5.6 nM, respectively). Three series of compounds were synthesized bearing different substituents at the C-2 position by replacing various amines at the C-4 position. Substituents at the C-2 position increased the enzymatic activity in this decreasing order:  $CH_3 > Cl > H$ . Also, it was observed

that the VEGFR-2 inhibitory activity was more accommodating towards the installation of bulky C-4 substituents. The results of these modifications on the kinase assay did not demonstrate any improvement in the activity of **12**, and their best effort was to introduce **13** (Fig. 12) as an equipotent compound for both inhibition of VEGFR-2 ( $IC_{50} = 8.4$  nM) and CAM (chorioallantoic membrane) angiogenesis assay. Nonetheless, examination of the cellular assay showed several compounds, such as **13**, with good activities on a number of tested cell lines, which could be attributed to their microtubule targeting properties as shown in **Table 6**. Evaluation of these compounds on  $\beta$ -III tubulin isotype and P-gp (P-glycoproteinATP-dependent drug efflux pump) overexpressing cell lines revealed that they could overcome  $\beta$ -III and P-gp mediated resistance compared to paclitaxel, a known substrate for P-gp (**Table 6**).

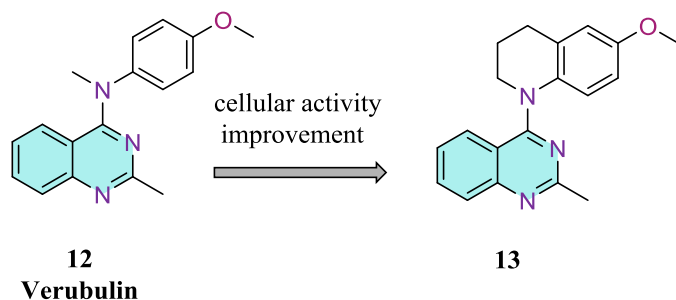


**Figure 12.** Structural representation of **12** and **13**.

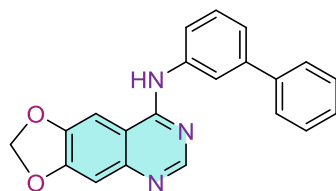
**Table 6**

Results of cellular evaluations of compounds **12** and **13**. (data extracted from (59))

Effect on Cell Viability ( $EC_{50}$ , nM)				
Compounds	Hela	Hela WT $\beta$ -III	SK-OV-3	SK-OV-3-MDR1-6/6
<b>12</b>	2.0	1.5	2.2	2.6
<b>13</b>	1.2	1.2	1.5	2.2
CA-4	3.3	3.3	5.5	7.2
Paclitaxel	2.8	24.0	5.0	1200

Conconi *et al.* introduced 6,7-fused dioxoquinazolinone derivative **14** (Fig. 13) with submicromolar inhibitory activity against different types of cell lines (**Table 7**) (61). This compound also inhibited various other angiogenesis-related kinases, including EGFR, FGFR-1, PDGFR- $\beta$ , and VEGFR-2, although **14** had the weakest inhibitory effect on VEGFR-2 ( $IC_{50} = 0.848$   $\mu$ M) as shown in **Table 8**. These results were supported by docking simulations of compound **14** revealing that terminal phenyl moiety had edge to face arene-arene interactions

with phenylalanine residue in the DFG-motif of mentioned kinases, however this interaction was not observed in VEGFR-2. The anti-angiogenic effects of **14** in these assays, along with the viability of HUVEC cells may suggest reduced toxicity upon normal endothelial cells. Daily intraperitoneal administration of 50 mg/kg of **14** significantly reduced the syngenic hepatocellular carcinoma tumour growth in Balb/c mice.



**14**

**Figure 13.** Structural representation of **14**.

**Table 7**

Results of cellular evaluations of compound **14**. (data extracted from (61))

Compound	Effect on Cell Viability (EC <sub>50</sub> , μM)						
	A431*	NIH3T3**	MCF-7 β	HT-29***	HeLa	BNL****	HUVEC
<b>14</b>	0.81	0.61	0.77	0.95	0.77	2.80	0.75

\*A431: Human epidermoid squamous carcinoma

\*\*NIH3T3 : Embryonic mouse fibroblast cell line

\*\*\*HT-29 : Human colorectal adenocarcinoma

\*\*\*\*BNL : Normal murine liver cell line

**Table 8**

Results of enzymatic evaluations of compound **14**. (data extracted from (61))

Compound	Inhibition Level (IC <sub>50</sub> , μM)					
	EGFR	FGFR-1	VEGFR-2	PDGFR β	Src	Abl
<b>14</b>	0.002	0.063	0.848	0.243	0.032	0.051

By merging the structures of icotinib and lapatinib, Xu *et al.* designed a series of quinazoline-based cytotoxic agents (62). Modifications on the crown ring sizes at C-6 or C-7 positions of the quinazoline skeleton and embellishing different substituents at the C-4 position led to compound **15** (Fig. 14) which selectively inhibited VEGFR-2 (compared to EGFR and PDGFR-β) with an IC<sub>50</sub> = 46.4 nM compared to sorafenib IC<sub>50</sub> = 140.6 nM). **15** exhibited broad-spectrum cytotoxic activity against Hep-G2, SH-SY5Y (neuroblastoma cell line), A549, MCF-7 and DU145 (human prostate cancer cells) cell lines, which in all cases had superior activity compared to those of reference drugs sorafenib and gefitinib. Based on the effects on MMP and

ROS production, it was indicated that compound **15** could induce apoptosis via a mitochondria-mediated apoptotic pathway, which was also confirmed by loss of original morphological features in Hep-G2 cells. Antitumour activity of compound **15** on the Hep-G2 xenograft mouse model revealed tumour growth inhibition in a dose-dependent manner which was comparable to sorafenib. Docking of compound **15** in the active site of VEGFR-2 (PDB code 1y6a) demonstrated the formation of two hydrogen bonds, one between NH of the anillino moiety and Asn1031 and another one between oxygen atom of benzyl moiety and Phe1045 residues.

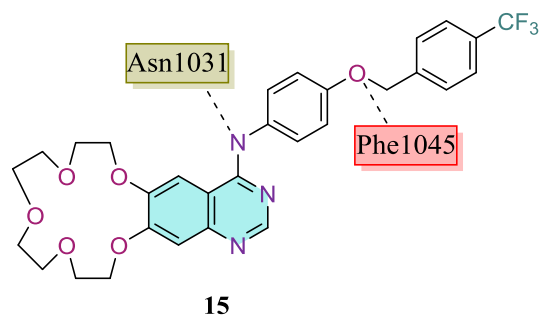


**Figure 14.** Structural representation of **15**.

Li *et al.* used *de novo* drug design method to discover novel quinazoline-based FLT-3 inhibitors, resulting in compound **16** (SKLB1002) (Fig. 15), which could inhibit 91% of this enzyme's activity (final concentration of 10  $\mu$ M) (63). Further studies on compound **16** revealed its inhibitory activity on VEGFR-2 ( $IC_{50}$  = 32 nM), in addition to downregulation of the downstream protein kinases (64). Examination of **16** on angiogenesis-related pathways in *in vitro* assays revealed an  $IC_{50}$  value of 11.9  $\mu$ M against V-HUVEC cell proliferation alongside inhibiting migration, invasion and tube-formation of these cells. **16** could block intersegmental vessels and microvasculature formation in zebrafish embryos in *in vitro* angiogenesis assessment. Administration of 100 mg/kg/d of **16** in Hep-G2 and SW620 (human colon adenocarcinoma) xenografts resulted in more than 60% tumour growth inhibition compared to the control group.

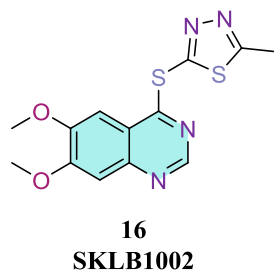




**Figure 15.** Structural representation of **16**.

### Functionalization of Quinazoline Core with Hydrogen Bond Donor/Acceptor Groups

Another strategy for designing VEGFR-2 inhibitors is the placement of various groups that can occupy a hydrogen bond rich region of the active site. This modification is done mainly by placing hydrogen bond donor/acceptor groups, typically linked to aromatic rings at the C-4 position of the quinazoline core. Urea moiety is the most frequent substituent; regardless, thiourea, amide semicarbazide, thiosemicarbazide (65), formylhydrazide and other moieties can represent similar binding interactions, typically resulting in type 2 inhibitors of the enzyme.

### Equipment of HB donor/acceptor groups at C-4 position

In a 2005 study, mostly based on quinoline derivatives, Kubo *et al.* reported 6,7-dimethoxy quinazoline derivative **17** (Fig. 16) containing 1,3-diphenylurea group, which exhibited great VEGFR-2 and PDGFR inhibition ( $IC_{50} = 2.2$  and  $3.6$  nM, respectively) (66).

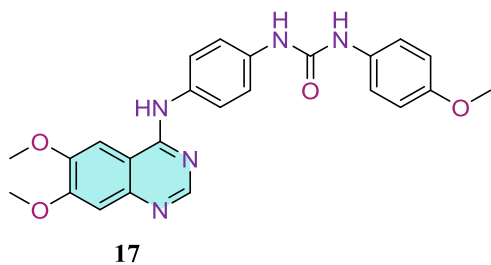


**Figure 16.** Structural representation of **17**.

In another work done by this research group, the quinazoline derivative **18** (KRN633) (Fig. 17) was introduced, which revealed to be highly selective against the VEGFR family (67). Accordingly, **18** had  $IC_{50}$  values of 170, 160, and 125 nM, against VEGFR-1, 2 and 3, respectively. Subsequently, compound **18** inhibited tyrosine phosphorylation of VEGFR-2 in HUVEC cells with an  $IC_{50}$  value of 1.16 nM. Additionally, **18** also inhibited the activation of mitogen-activated protein kinases (ERK1 and ERK2) by VEGF, along with a block on HUVEC proliferation and tube formation. The oral administration of this compound inhibited tumour growth (in some cases TGI > 100%) in athymic mice and rats modelled with tumour xenografts

of various tissue origins, such as lung, colon, and prostate, with no substantial effect on the body weight of the animals. Histological assessment of **18** in treated tumours showed a decrease in vascular permeability and tumour vessel formation. Compound **18** also presented a suitable pharmacokinetic profile and in vivo efficacy.

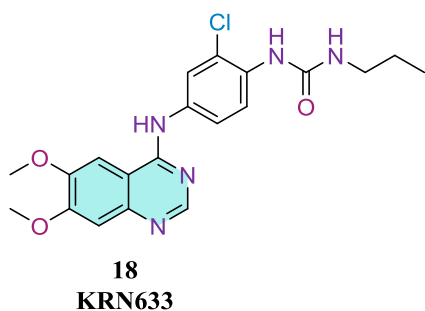


**Figure 17.** Structural representation of **18**.

Garofalo *et al.* synthesized several compounds by inserting urea, carbamic acid ester, or amide groups linked to the C-4' position of the anilinoquinazoline scaffold (68). These compounds are multi-target-directed-ligands (MTDLs), a family of compounds described as promising tools to tackle complex diseases (69). Comparing these groups, amide derivatives did not have the desired inhibitory activity, carbamate counterparts presented a dual EGFR/VEGFR-2 activity, and urea derivatives had the best VEGFR-2 inhibition. In addition, the replacement of one of the methoxy groups with a diethylaminoethoxy at the C-6 or C-7 positions of the quinazoline ring evidently decreased the activity. Among them, **19** (Fig. 18) containing carbamic acid methyl ester group demonstrated  $IC_{50}$  values of 6.87 and 5.79  $\mu\text{M}$  against EGFR and VEGFR-2 kinases, respectively, although it had weak inhibitory activity towards hormone-independent PC3 prostate cancer cells. Compound **20** (Fig. 18) presented an  $EC_{50}$  value of 8.8  $\mu\text{M}$  against PC3 cells accompanied by an acceptable VEGFR-2 inhibition ( $IC_{50} = 5.12 \mu\text{M}$ ).

Further investigations were based on compound **19** to exceed their inhibitory activity (70). The addition of methyl or chlorine to C-3' and C-5' of the aniline moiety resulted in submicromolar dual inhibitory activity of target compounds. The carbamic acid ester group is better tolerated in C-4' rather than C-3' (compound **21** (Fig. 18)). The addition of morpholinoethoxy or piperidinoethoxy in the C-7 of the 4-anilinoquinazoline skeleton led to a significant loss of EGFR activity while increasing potency against VEGFR-2 (compound **22** (Fig. 18)). As mentioned, **21** demonstrated  $IC_{50}$  values of 0.5 and 1  $\mu\text{M}$  compared to compound **22** with 0.3 and 8.5  $\mu\text{M}$  against VEGFR-2 and EGFR, respectively. Despite observing decent enzymatic activity

in some compounds, nearly all were poorly cytotoxic against PC3, HT-29 (human and MCF-7 cancerous cell lines). Docking study of compound **21** revealed an interaction between the carbonyl group of the carbamate entity with Asp1046 and NH of the carbamate group with Glu885 residue in the active site of VEGFR-2. Also, another hydrogen bond interaction was between N-1 of the quinazoline core and NH of Cys919, located in the hinge region.

Continuing with this study, by further explorations on compound **20**, Garofalo *et al.* reported novel aryloxy-linked quinazolines as selective VEGFR-2 inhibitors (71). Replacement of NH with N-methyl entity at the C-4 position of the quinazoline core dramatically decreased VEGFR-2 inhibition, but inserting Oxygen at the C-4 enhanced the activity. Compounds with the urea functionality on the C-4' position were 10-fold more potent than their C-3' analogues. The most potent VEGFR-2 inhibitor, **23** (Fig. 18) displayed an  $IC_{50}$  value of 0.03  $\mu$ M, and compound **24** (Fig. 18) had the best inhibitory effect against angiogenesis-related cell line, human endothelial-like immortalized EAhy926 cells ( $IC_{50} = 5 \mu$ M), accompanied by an  $IC_{50}$  value of 0.06  $\mu$ M against VEGFR-2.

Considering previous modifications Garofalo and colleagues surmised that substitution of methyl or halogen on the phenyl ring linked to C-4 of the quinazoline core appeared to increase the enzymatic activity; however, despite their intense activity against VEGFR-2, they did not reflect a decent antiproliferative activity on cell-based assays due to poor solubility (72). The most potent compounds were **25** and **26** (Fig. 18), exhibiting  $IC_{50}$  values of 4 and 2 nM against VEGFR-2, respectively. For further development, docking and 3D QSAR models employing the CoMFA and CoMSIA methods were conducted, elaborating excellent predictive power and validating the hypothesis of binding mode for biological evaluations.

In subsequent studies based on **25** and its analogues, further modifications were applied by Ravez *et al.* to improve enzymatic and cellular activities, therefore, a series of 7-aminoalkoxy-4-aryloxy-quinazoline ureas were synthesized (73). Modification of the methoxy group at the C-7 position by adding an aminoalkyl basic side chains revealed a range of potent inhibitors of the VEGFR family, PDGFR- $\beta$  and c-Kit kinases, which could significantly inhibit cell proliferation in PC3, HT-29, MCF7 cancer cell lines and HUVEC whereas lowering proliferation inhibition against the normal cells MRC5 (human fetal lung fibroblast cells), as shown in **Table 9**. Similar values were obtained in the assessment of HUVEC inhibition, by changing the nature of the amine (diethylamino-, piperidino-, pyrrolidino- moiety) or the length of the linker (ethoxy or

propoxy). Compound **27** (Fig. 18) was introduced as a potent ATP-competitive multi-kinase inhibitor with  $IC_{50}$  values below 10 nM against VEGFR-(1, 2 and 3), PDGFR- $\beta$  and c-Kit (**Table 9**), with lower concentrations than the reference, cediranib, it strongly suppresses angiogenic processes by inhibiting the invasion of HUVEC endothelial cells in a dose-dependent manner and preventing the formation of tubes in endothelial tube formation assay.

In another study in 2015, Ravez and coworkers designed different bicyclic pyrimidine scaffolds, such as the quinazoline core with or without substituents at C-6 or C-7 positions and several anilino or aryloxy groups at the C-4 position (74). Notably, compounds with diarylurea moiety showed the best VEGFR-2 and c-Kit inhibitory activity, introducing compounds **28** and **29** (Fig. 18) as multi-kinase inhibitors with  $IC_{50}$  values in the nanomolar range against several kinases, as shown in **Table 10**. Further inspections on antiproliferative activity against PC3, MCF7 and HT-29 (human colorectal adenocarcinoma cell line with epithelial morphology) revealed no or low inhibition at 10  $\mu$ M concentration.

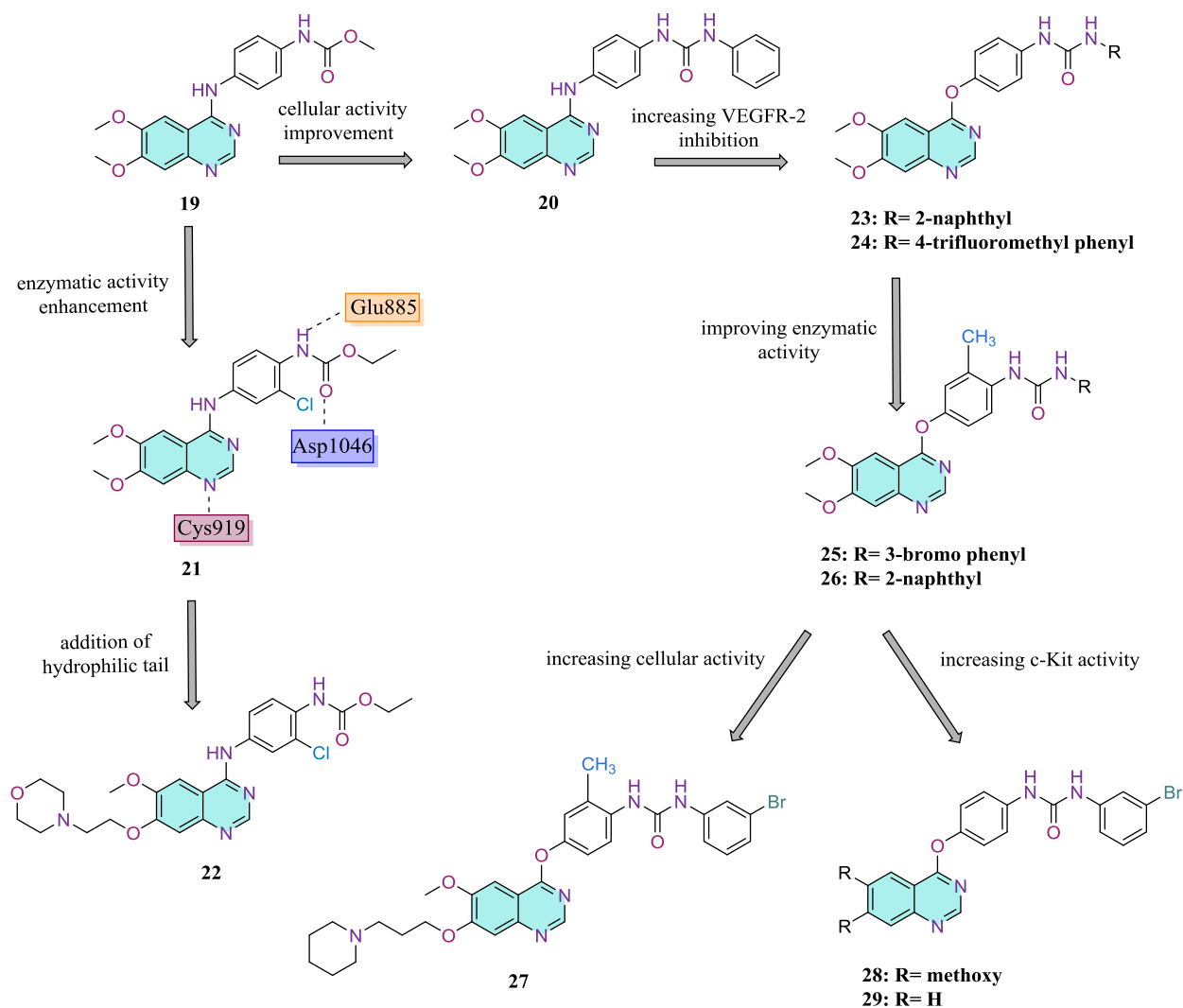


**Figure 18.** Structural representation of 19-29 and binding mode of 21 into VEGFR-2 active site.

**Table 9**

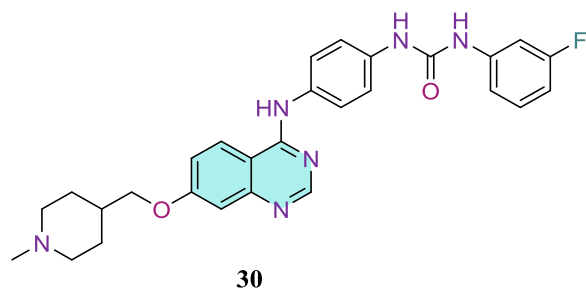
Results of biological evaluations of compound 27. (data extracted from (73))

	Inhibitor Level (IC <sub>50</sub> , μM)				Effect on Cell Viability (EC <sub>50</sub> , μM)				
	VEGFR-1	VEGFR-2	VEGFR-3	PDGFR-β	c-Kit	PC3	HT-29	MCF7	HUVEC
<b>27</b>	5	4	8	9	9	4.09	1.00	5.02	0.33
<b>vandetanib</b>	150	69	260	5300	-	7.30	1.76	9.57	4.39
<b>cediranib</b>	39	14	11	38	1530	>10	1.61	7.94	0.27

**Table 10**Results of enzymatic evaluations of compounds **28** and **29**. (data extracted from (74))

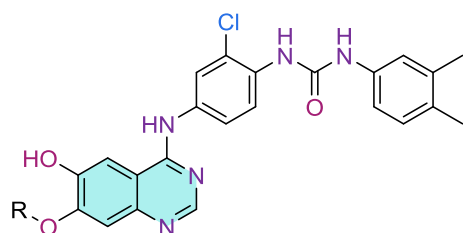
Compounds	Inhibitor Level (IC <sub>50</sub> , nM)				
	VEGFR-1	VEGFR-2	VEGFR-3	PDGFR-β	c-Kit <sub>wt</sub>
<b>28</b>	46	6	9	5	16
<b>29</b>	650	8	7	320	14

Yu and colleagues introduced a series of 4-anilino quinazoline derivatives based on vandetanib (75). Their SAR study revealed that the insertion of the basic (1-methylpiperidin-4-yl)methoxy group at C-7 position of the quinazoline core improved the solubility of the compounds. At the C-2' position of the aniline ring, the placement of chlorine and fluorine atoms decreased the activity. As a linker between aniline ring and terminal groups, urea was preferred over acetamide moiety. Compounds bearing aromatic terminal groups revealed better inhibitory activity than those with aliphatic groups such as cyclopropyl or ethyl. The most potent compound **30** (Fig. 19) with terminal 3-F phenyl group demonstrated selective inhibition against VEGFR-2 (IC<sub>50</sub> = 5.5 nM) and VEGFR-3 (IC<sub>50</sub> = 9.6 nM) compared to VEGFR-1, EGFR, FGFR-1 and Tie-2. Additionally, it demonstrated good antiproliferative potency against V-HUVEC with an IC<sub>50</sub> of 52 nM, which was more potent than its counterparts containing methoxy groups at C-6. In vivo evaluation of **30** in the Hep-G2 cells xenograft model, with once-daily oral administration at three doses for 15 days, revealed a tumour growth inhibition of 83.6% at 100 mg/kg dosage.

**Figure 19.** Structural representation of **30**.

Zhang and colleagues provided substituted diaryl urea or glycine methyl ester groups instead of the anilino moiety at the C-4 position of the quinazoline ring as dual EGFR and VEGFR-2 inhibitors (76). Eventually, diaryl urea derivatives showed better cellular and enzymatic activities than their counterparts containing glycine methyl ester. Investigating the effect of side chains at the C-7 position, different substituents containing 4-methyl piperazine, morpholine,

piperidine and benzyloxy were examined. Among the different levels of activity of the tested compounds, the benzyloxy side chain significantly reduced both enzymatic and cellular activities. Insertion of a Chlorine atom in the *ortho*-position of the urea moiety dramatically increased EGFR and VEGFR-2 kinase inhibition. Compound **31** (Fig. 20) had the highest VEGFR-2 inhibitory activity with a  $IC_{50}$  value of 14 nM, accompanied by an  $IC_{50}$  value of 51 nM against EGFR. Interestingly, compound **32** (Fig. 20) with an acceptable EGFR and good VEGFR-2 inhibition (817 and 18 nM, respectively) displayed the best antiproliferative activity. (**31** and **32** cellular inhibition profile is shown in **Table 11**).



**31:** R= 4-propylmorpholine  
**32:** R= 1-ethylpiperidine

**Figure 20.** Structural representations of **31** and **32**.

**Table 11**

Results of cellular evaluations of compounds **31** and **32**. (data extracted from (76))

Compounds	Effect on Cell Viability ( $EC_{50}$ , $\mu$ M)		
	HT-29	MCF-7	H460*
<b>31</b>	7.29	2.63	3.52
<b>32</b>	1.85	1.27	2.90
<b>Vandetanib</b>	18.95	11.83	37.10

\*H460: non-small cell lung cancer cell line

Following the 2016 study designing EGFR inhibitors (77), an attempt was made on cyclization at 5,6 positions of quinazoline ring, to introduce novel diaryl urea [1,4]dioxino[2,3-f]quinazoline-based VEGFR-2 inhibitors (78). According to their SAR analysis, placement of phenyl ring as a linker between urea moiety and quinazoline core was preferable to pyridyl. Also, the insertion of halogen atoms at C-2' and C-3' was tolerated. Most of the compounds revealed  $IC_{50}$  values under 10 nM against VEGFR-2. It is worth noting that the introduction of different hydrophilic groups on the C-7 position of the quinazoline ring showed no significant difference between the counterparts bearing methoxy at this position. Compound **33** (Fig. 21) was the most potent in the

enzymatic assay, with an  $IC_{50}$  value of 1.0 nM. All compounds manifested profound antiproliferative activity against V-HUVEC in which  $IC_{50}$  values were lower than 5 nM. Moreover, to evaluate their safety profile, compounds were tested against human renal epithelial HEK293 and normal human hepatocytes LO2 cell lines. Most compounds possessed  $IC_{50}$  values of more than 1000 nM, presenting great selectivity. Accordingly, compound **34** (Fig. 21) was chosen for further evaluations against human hepatoma cells SMMC7721, displaying an  $IC_{50}$  value of 375.5 nM. Also, with 60 mg/kg OD dosing of **34** for six days in an *in vivo* model of SMMC7721 inoculated nude mice, tumour growth was greatly inhibited with a TGI value of 133.0%. Molecular docking studies (PDB code 3WZD) showed a similar binding pattern between **34** and lenvatinib, with key interactions of N-1 of the quinazoline nucleus with Cys919, and urea moiety with Glu885 and Asp1046. The ethylenedioxy segment extended to the hydrophobic region of VEGFR-2 pocket.

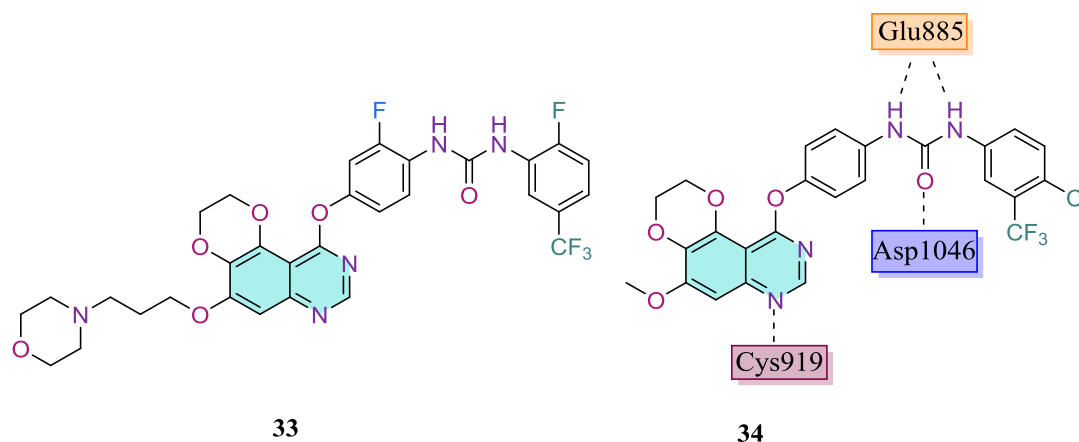


**Figure 21.** Structural representation of **33** and **34** and key interactions of **34** with VEGFR-2.

Abd El Hadi *et al.* designed a series of quinazoline-based VEGFR-2 inhibitors incorporating ester or carboxamide functional groups at the C-2 position (79). SAR analysis indicated that carboxamide is preferable to the ester group; also, the insertion of the Fluorine atom on the C-3' position enhanced the VEGFR-2 inhibition percentage. Placement of various substituents on the terminal phenyl ring led to compound **35** (Fig. 22) with the highest VEGFR-2 inhibition with an  $IC_{50}$  value of 12.1 nM. Analysis of sixteen selected compounds against the NCI-60 cell panel revealed that none of them had an acceptable cell inhibition rate, with the highest mean GI%



being 10.26%. Molecular docking of compound **35** embedded in the active site of VEGFR-2 (PDB code 4ASD), showed two hydrogen bonds simultaneously between Cys919 with NH of the carboxamide moiety and N-1 of the quinazoline core, also the urea fragment had two interactions with Glu885 and Asp1046 residues.

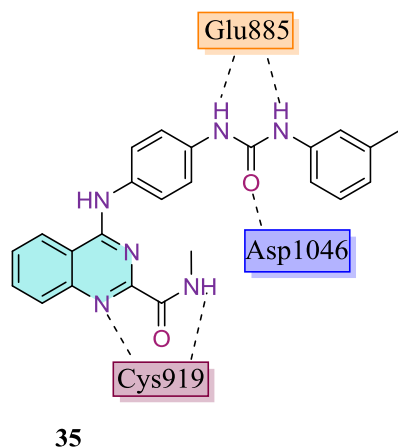


**Figure 22.** Structural representation of **35** and key binding interaction with VEGFR-2.

Zhang *et al.* used an experimental and computational approach based on BREED methodology employing their library and KLIFS as a database to identify a series of novel VEGFR-2 inhibitors bearing naphthalenyloxy entity at C-4 position of the quinazoline ring (80). A naphthalene ring was used instead of the phenyl moiety, which regularly occupies the hydrophobic region I in quinazoline-based VEGFR-2 inhibitors. Nearly all the compounds could inhibit VEGFR-2 by more than 95% in 10  $\mu$ M concentration. Compound **36** (Fig. 23), with the best enzymatic inhibition against VEGFR-2 and the remarkable  $IC_{50}$  value of 0.75 nM, did not have an acceptable inhibition rate on the MDA-MB-435 (Human melanoma cells) cell line. To expand the evaluation of anticancer cellular inhibition profile, compounds **37,38** and **39** (Fig. 23) ( $IC_{50}$  values against VEGFR-2, 15.29, 8.70 and 33.36 nM, respectively), which revealed favorable activity on MDA-MB-435 and HUVEC cell lines, were submitted to the NCI-60 platform. Among them, compound **39** showed significant antiproliferative activity against 51 out of 58 tested cell lines reducing the growth percentage to less than 50%. Compared to reference drugs sunitinib and sorafenib, which have FDA approval in the treatment of renal cell carcinoma, compound **39** exhibited lower  $GI_{50}$  and TGI values and higher  $LC_{50}$  value, indicating that it is more potent in cell lines responsible for renal cancer accompanied with a comparable safety for

clinical usage. As one of the cell lines tested, NCI/ADR-RES is a multidrug-resistant cancer cell line for ovarian cancer; compound **39** demonstrated GI<sub>50</sub> values of 3.4 and 6.9 times better than sorafenib and sunitinib, respectively. Further investigations on kinome screening indicated that compound **39** had multitargeted kinase activity, inhibiting 56 out of 349 targets greater than 90% (at 0.5 μM concentration), about two third of which have a high degree of sequence similarity to VEGFR-2. Docking studies showed hydrogen bond interaction between N-1 of quinazoline core with NH of Cys919 residue, other hydrogen bonds were between urea moiety and key residues of Glu885 and Asp1046. This result supported the initial pharmacophoric hypothesis that bicyclic groups (naphthalene) are fitted to hydrophobic region I better than monocyclic groups.

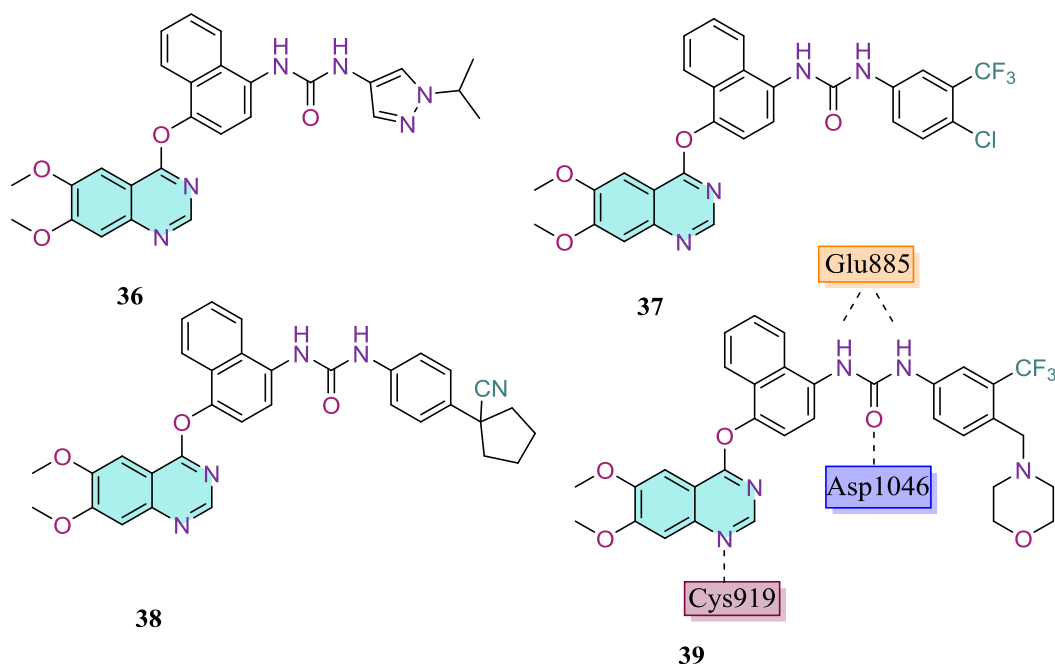


**Figure 23.** Structural representation of **36-39**, binding mode of **39** into VEGFR-2 active site.

In their previous study, Elsayed *et al.* developed a series of indazole-based VEGFR-2 inhibitors linked to the pyrimidine core (81). Following that, with a conformational rigidification strategy applied to compound **40** (Fig. 24), a new series of indazole-based VEGFR-2 compounds were introduced, replacing quinazoline as a hinge binder instead of the pyrimidine ring (82). Initially, the N-1 of the urea group was incorporated into an indazole moiety attached to quinazoline with an NH linker, leading to compounds with weak to moderate inhibitory activity against VEGFR-2. The second approach was orienting the indazole ring, thus connecting it from N-1 directly to the quinazoline core, which led to development of compounds with potent VEGFR-2 inhibition.

It was clear that the presence of 6,7 quinazoline tails and also insertion of substituents with optimal size (2-chloro-3-methyl for **41** (Fig. 24) and 3,4-dichloro for **42** (Fig. 24)) notably improved the potency. As mentioned, compounds **41** and **42** were superior in anti-VEGFR-2 activity with IC<sub>50</sub> values of 5.4 and 5.6 nM. Assessment of compounds **41** and **42** on HUVEC cells revealed 80% and 98% of inhibition, respectively at a concentration of 10 μM. Using the NCI-60 panel, the antiproliferative activity of **41** and **42** were investigated. The mean percentage of growth inhibition for **41** against all tested cell lines was 8%, except 74% against colon cancer cell line KM12 at a concentration of 10 μM. Compound **42** exerted significant potency against the full panel of cell lines, with a mean GI<sub>50</sub> of 130%. Additionally, **42** exhibited nanomolar GI<sub>50</sub> values against KM12 and human gliosarcoma cell line SF-539 (50 and 612 nM, respectively). Interestingly, GI<sub>50</sub> value against multi-drug resistant ovarian cancer cell line NCI/ADR-RES of **42** was better than sorafenib, maintaining an excellent safety profile (LC<sub>50</sub>>100 μM). Compound **42** was further chosen for the evaluation of independent angiogenic functionality against prostate cancer cell line PC-3, which is resistant to VEGFR-2 inhibitory therapy. Phosphorylation of Akt and ERK were reduced in cells treated with **42** compared to the control. In assessing the pro-apoptotic effect, **42** also increased caspase-3 activity three times more than the control. Comparing **42** with lenvatinib and tivozanib, it was observed that **42** is a type II inhibitor with hydrogen bonds between the urea moiety and both Glu885 and Asp1046 residues, as well as N-1 of the quinazoline ring with Cys919 residue.

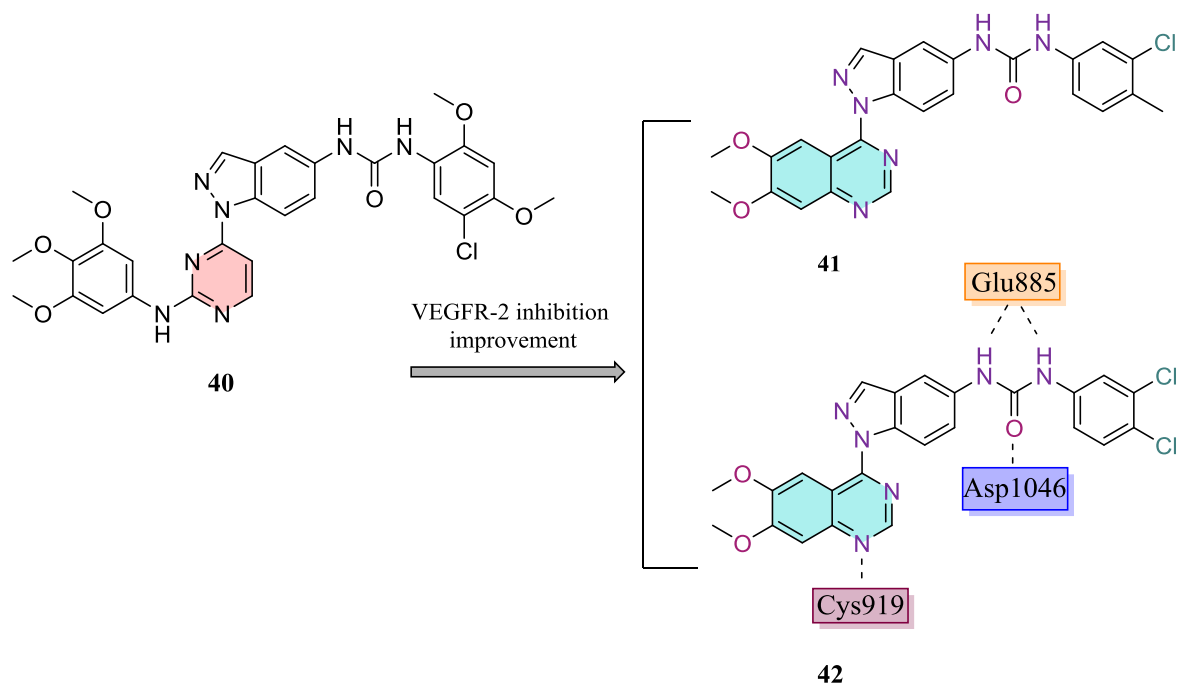


**Figure 24.** Structural representation of **40-42**, binding mode of **42** into VEGFR-2 active site.

In an attempt to enhance the potency and oral bioavailability of sorafenib, Potashman *et al.* designed lead compound **43** (Fig. 25) by cyclization of the urea moiety to achieve conformational rigidity while maintaining hydrogen bonding between Nitrogen atoms of the pyridine ring with the Cys-919-NH and amide-NH with amide-CO of Cys-919 in the kinase hinge region (83). Unexpectedly this alteration led to a decrease in both cellular activity and enzyme inhibition. A number of compounds were designed with benzimidazole, or benzoxazole rings, attached to a variety of heterocyclic cores to improve the cellular potency of compound **43**; among them, quinazoline-based compounds **44** and **45** (Fig. 25) were obtained. Compounds **44** and **45** were found with  $K_i$  phos of 8 and 0.5 nM against VEGFR-2, respectively. **44** displayed an  $IC_{50}$  value of 49 nM against V-HUVEC, and in the evaluation of kinase selectivity profile, **45** also displayed an  $IC_{50}$  value of 6 nM against V-HUVEC compared to an  $IC_{50}$  value of 55 nM F-HUVEC. In the study of in vivo pharmacokinetic parameters in male Sprague-Dawley rats, compound **45** exhibited an acceptable profile with 60% bioavailability.

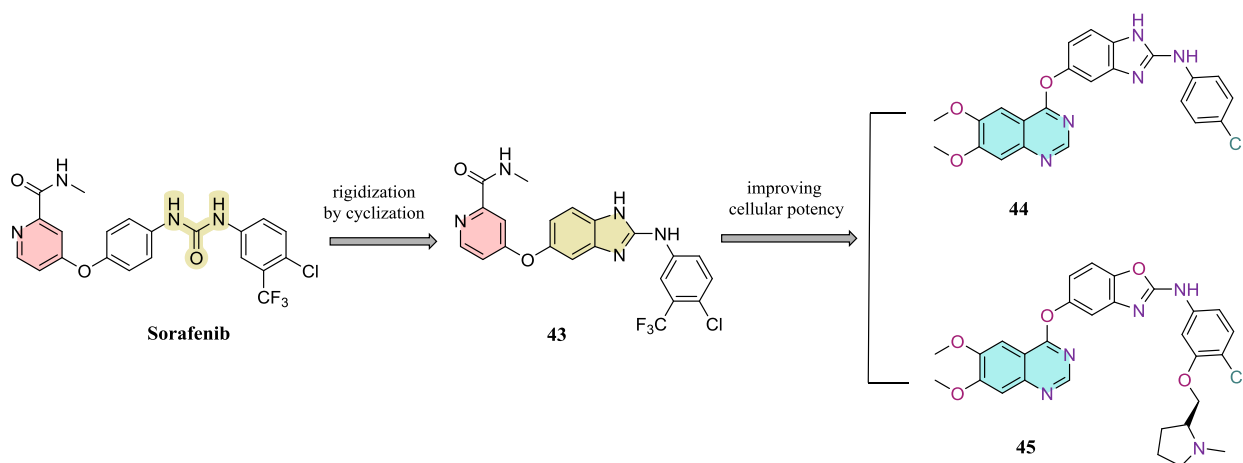


**Figure 25.** Structural representation of sorafenib and compounds **43-45**.

c-Met kinase function has been shown effective in collaboration with VEGFR-2, implicating that inhibition of c-Met significantly improves VEGFR-2's blockage effect on angiogenesis and cancer progression. In this manner, Shi *et al.* introduced a series of quinazolin-4-amines bearing benzimidazole moiety as dual c-Met and VEGFR-2 inhibitors (84). SAR analysis revealed that small electron-withdrawing substituents on the phenyl ring attached to 2 position of the benzimidazole were favourable for cellular and enzymatic activities. In the antiproliferation assay, almost all compounds had better activities against MCF-7 than Hep-G2. Compound **46** (Fig. 26) with 4-F substituent exhibited the most potent inhibitory activity against c-Met and VEGFR-2 with  $IC_{50}$  of 0.05  $\mu$ M and 0.02  $\mu$ M, respectively, accompanied with the best cellular activity against MCF-7 and Hep-G2 with  $IC_{50}$  values of 1.5  $\mu$ M and 8.7  $\mu$ M, respectively surpassing reference drug golvatinib (49.6 and 65.5  $\mu$ M, respectively). Docking studies (PDB code 2QU5) showed hydrogen bonds forged between the nitrogen atom linked to C-4 of quinazoline ring and Glu885 along with the fluorine atom and Cys919.

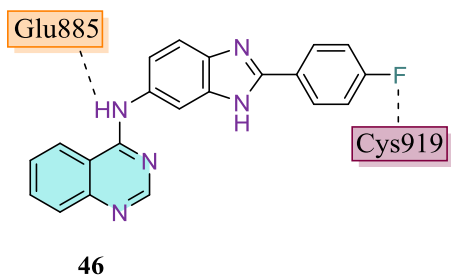


**Figure 26.** Structural representation and binding mode of **46** towards VEGFR-2.

Researchers from AstraZeneca introduced a novel series of quinazolines possessing acetanilide substituted pyrazole ring at C-4, which led to clinical candidate, baracertib (AZD1152) **47** (Fig. 27), showing great activity against the Aurora family of kinases (85). Plé *et al.* modified these series to improve their activity against PDGFR $\beta$  and VEGFR-2 (86). First, they synthesized compound **48** (Fig. 27), inhibiting VEGFR-2 with an IC<sub>50</sub> value of 0.8 nM with a great enzymatic profile as shown in **Table 12**. The replacement of Nitrogen instead of Oxygen atom in C-4 position of the quinazoline ring reduced the activity. The activity against VEGFR-2 was diminished by substitution at C-5 position. Insertion of neutral or basic side chains in C-6 or C-7 positions maintained the activity, but compounds with basic side chains suffered from an unacceptable pharmacokinetic profile. Despite its great potency, compound **48** had some drawbacks, such as relative instability in acidic conditions and poor bioavailability. Placing the phenyl ring instead of pyrazole improves chemical stability and pharmacokinetic profile while maintaining the same inhibitory activities. As with the pyrazole series, the C-4 aminoquinazolines were considerably less potent than the corresponding ethers. The addition of a side chain to the *meta* position of the phenyl ring rather than the *para* position, as well as the replacement of the *para*-acetanilide with urea, sulfonamide, reversed amide, or benzamide, reduced the activity. Among the diverse lipophilic groups introduced on the right-hand side of acetanilide moiety, pyrazoles were the most potent series. All these modifications led to compound **49** (AZD2932) (Fig. 27) exhibiting a significant VEGFR-2 inhibitory activity with an IC<sub>50</sub> value of 8 nM (kinase inhibition profiles are represented in **Table 12**). The DMPK profile of compound **49** in rats and dog were investigated extensively. The bis-(dihydrogenphosphate) salt of **49** provided a 15-fold increase in dissolution rate over the free base to improve pharmacokinetics. The DMPK parameters of **49** in the salt form examined in dog is presented in **Table 13**. Continuing with this study, Kettle *et al.* reported a series of pan-KIT inhibitors in an attempt to lower VEGFR-2 affinity (87). Among the synthesized compounds, compound **50** (Fig. 27) had an IC<sub>50</sub> value of 442 nM against VEGFR-2. The critical interactions of **50** bound to the kinase domain of VEGFR-2 was obtained by the X-ray crystallography exhibiting binding of the isopropyl group to the DGF pocket and three hydrogen bonds, one between N-1 of the quinazoline with the hinge region, another two between the nitrogen of the amide functionality and Glu885 and oxygen of the carbonyl with Asp1046, while the two methoxy groups occupied the solvent region.

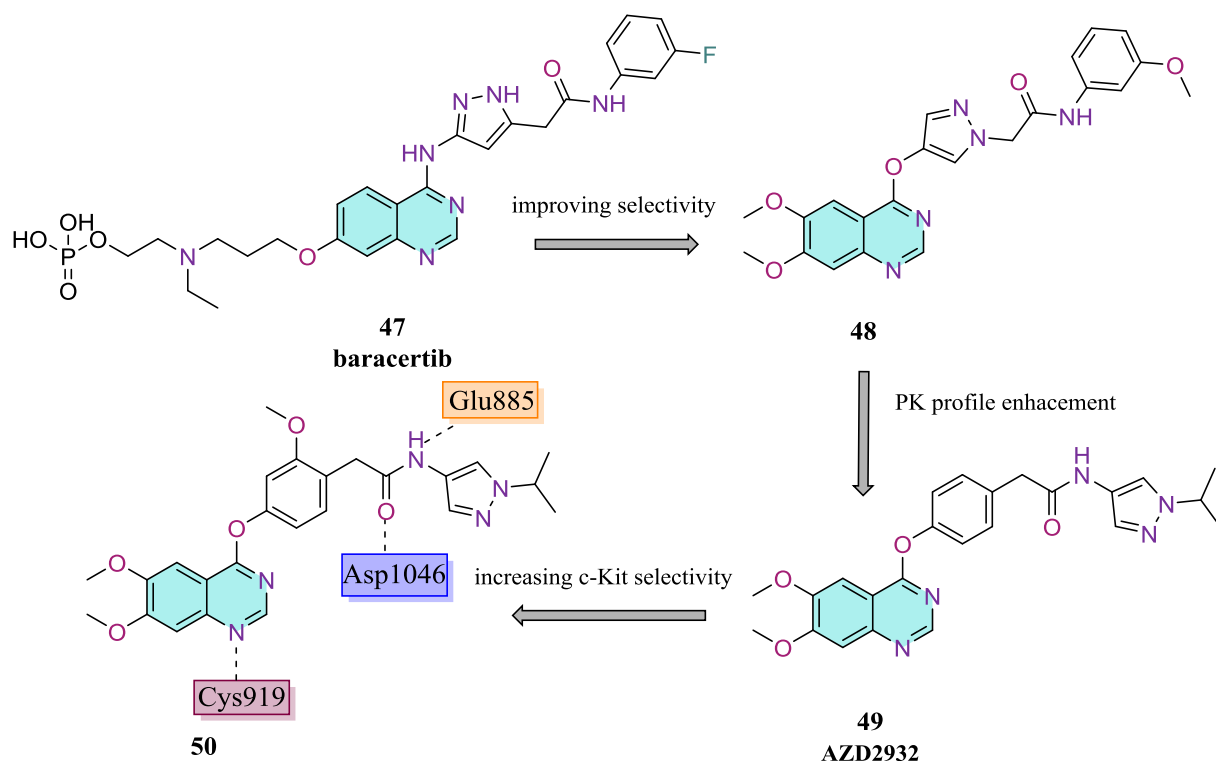


**Figure 27.** Structural representation of **47-50** and binding mode of **50** into VEGFR-2 active site.

**Table 12**

Results of enzymatic evaluations of compounds **48** and **49**. (data extracted from (86)).

Compounds	Inhibition Level (IC <sub>50</sub> , nM)			
	VEGFR-2	PDGFR β	CSF-1R	FLT-3
<b>48</b>	0.4	0.8	10	2
<b>49</b>	8	4	100	7

**Table 13**

PK profile of compound in dog **49** (data extracted from (86)).

Compound	Dose (mg/kg)	Cl (ml/min/kg) % HBF	V <sub>dss</sub> (l/kg)	PO t <sub>1/2</sub> (h)	IV t <sub>1/2</sub> (h)	F (%)
<b>49</b>	3 (iv)	1.7 (iv)	0.7	4.7	6.8	>90
	10 (po)	5.2 (po)				

Zhang *et al.* synthesized 4-anilinoquinazoline derivatives containing acylamino moiety as dual-acting inhibitors against EGFR and VEGFR-2 (88). Among different chains at C-7 position of the quinazoline ring, compounds containing 4-methyl piperazine showed better inhibitory activity compared to their piperidine and morpholine counterparts. Benzylloxy significantly reduced both cellular and enzymatic activities. The best VEGFR-2 inhibitory activity was

exhibited in compound **51** (Fig. 28) with an  $IC_{50}$  value of 0.56  $\mu\text{M}$ , accompanied by an  $IC_{50}$  value of 0.13  $\mu\text{M}$  against EGFR. However, **51** exhibited weak antiproliferative activity on three types of cancer cell lines. Additionally, compound **52** (Fig. 28) with  $IC_{50}$  values of 1.81 and 0.15  $\mu\text{M}$  against VEGFR-2 and EGFR, respectively, exhibited the best cellular activity with  $IC_{50}$  values of 5.27, 4.41 and 11.95  $\mu\text{M}$  against HT-29, MCF-7 and H46, respectively. Docking studies (PDB code 2OH4) showed that compound **51** accommodates to DFG-out conformation of VEGFR-2 via hydrogen bonds between N-1 of quinazoline with Cys917, oxygen atom from carbonyl group with Asp1044 and also NH of the acylamino group with Glu883. Additionally, The methoxy at C-6 position interact with two NHs of Arg1049 residue.

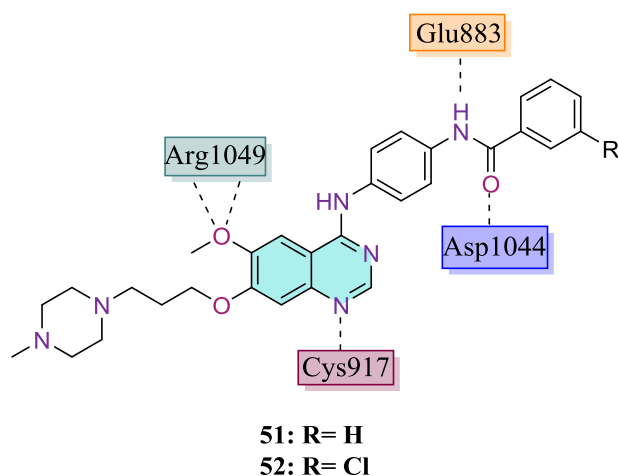


**Figure 28.** Structural representation of **51** and **52** and schematic representation of key interactions from **51** and **52** inside the VEGFR-2 active site.

Wang *et al.* synthesized 6,7-dimethoxy quinazoline-based agents bearing diarylamide moiety as novel VEGFR-2 inhibitors. According to the SAR studies, different positions on the terminal phenyl ring increase potency in the following order: *meta* > *para* > *ortho*. Generally, small lipophilic groups such as halogens were preferable for both cellular and enzymatic activities and the activities were lined as  $F > Cl > I$ ; indeed, the highest activity was observed with a methyl substituent. Compound **53** (Fig. 29) exhibited the most potent VEGFR-2 inhibition with an  $IC_{50}$  value of 16 nM, along with the best cellular activity against Hep-G2 and MCF-7 cell lines. ( $IC_{50}$  values 7.5 and 13  $\mu\text{M}$ , respectively). Molecular docking of compound **53** (PDB code 3B8Q) revealed two conventional hydrogen bonds including N-1 of quinazoline core with Cys919 and



NH of the amide moiety with Oxygen atom of Asp1046 in the ATP binding site of VEGFR-2.  
(89)

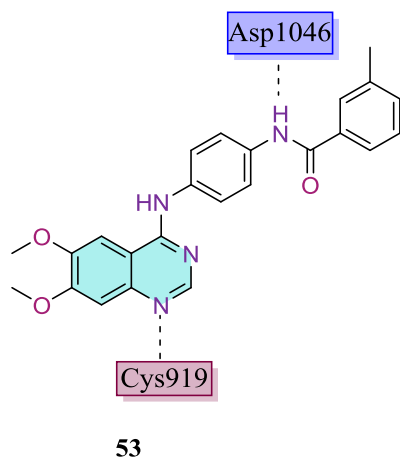


**Figure 29.** Structural representation of **53** and schematic representation of key interactions from **53** inside VEGFR-2 active site .

In another work, E. Abdallah *et al.* investigated three series of compounds with different core scaffolds, such as quinazoline, quinoxaline and nitrobenzene, with an assumption that they bind to the ATP binding domain of VEGFR-2 (90). The quinazoline nuclei exhibited superior activity with  $IC_{50}$  values ranging from 60 to 94.22 nM versus VEGFR-2. Compound **54** (Fig. 30) had the highest inhibition against VEGFR-2 ( $IC_{50}$  = 60 nM), alongside an acceptable selectivity against HER-2 and FGFR enzymes. **54** revealed  $IC_{50}$  values of 24.10, 40.90 and 33.40  $\mu$ M versus Hep-G2, PC3 and MCF-7 cell lines with an acceptable selectivity against WI-38 normal human fibroblast cell line. Investigation of **54** on apoptotic markers showed a lowering in Bcl-2 levels and a raise in proapoptotic Bax and P53 levels and also caspase-3 activation. Docking simulation of **54** (PDB code 4ASD) showed that it was able to interact with the critical amino acids in the same way as sorafenib, resulting in an interaction between chlorine atom and Cys919, and the amide moiety with Glu885 and Asp1046 residues.

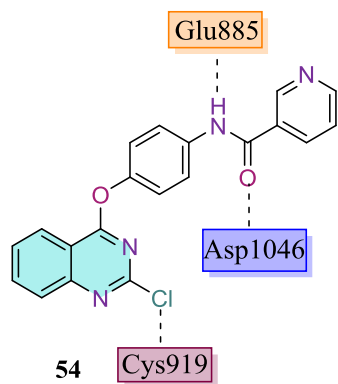


**Figure 30.** Structural representation and binding mode of **54** into VEGFR-2 active site.

Ashok and coworkers introduced a series of 6,7-dimethoxy quinazoline derivatives bearing 3-amino-thiophene-2-carboxamide at the C-4 position (91). Substitution of aryl groups in the carboxamide position led to compound **55** (Fig. 31) with the highest enzymatic inhibitory activity against both VEGFR-1 and VEGFR-2 with  $IC_{50}$  values of 0.11 and 0.087  $\mu\text{M}$ , respectively. The placement of cycloalkyl groups in this position significantly diminished potency against both enzymes .

Following their previous work, they altered the thiophene ring with 4-amino nicotinamide moiety at the C-4 position (92). Compound **56** (Fig. 31) bearing thiophene-2-yl methyl at the amidic position exhibited the highest VEGFR-2 inhibition with a remarkable  $IC_{50}$  value of 17 nM. Similarly, the substitution of aryl groups at the amidic position alleviated the enzymatic activity.

In another project, Ashok *et al.* synthesized 4-anilino-6,7-dimethoxy quinazoline containing 1,2,4-oxadiazole derivatives (93). Investigation of enzymatic inhibition in an HTRF assay revealed that compound **57** (Fig. 31) exhibited the most potent inhibitory activity against VEGFR-2 with an  $IC_{50}$  value of 17 nM and also showed 91% inhibition against VEGFR-1 at 10  $\mu\text{M}$  concentration.

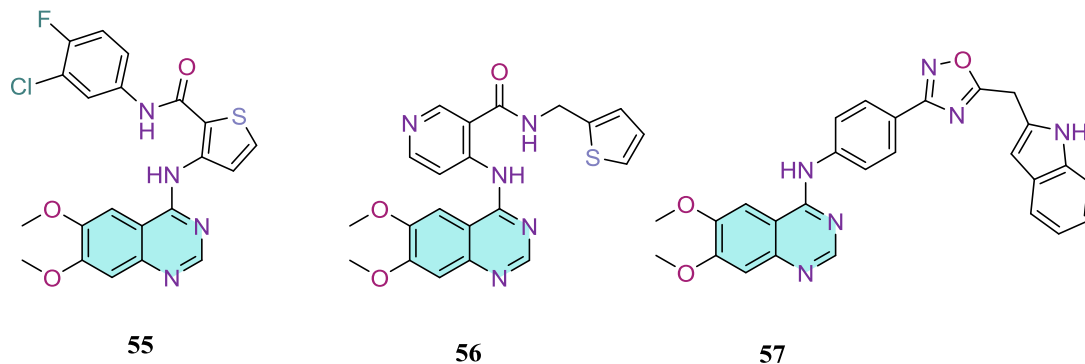
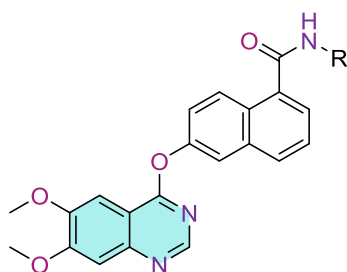


**Figure 31.** Structural representation of **55-57**.

According to Amgen studies, a series of naphthamides were introduced and further evaluated as novel VEGFR-2 inhibitors (94). This study showed that compounds with a quinoline core had the most promising inhibitory activities, although corresponding quinazolines were also potent VEGFR-2 inhibitors. Compounds **58** and **59** (Fig. 32) showed remarkable  $IC_{50}$  values of 2.9 and 1.3 nM against VEGFR-2, respectively as well as 7.3 and 16 nM against V-HUVEC, respectively. They were also selective against other kinases angiogenesis-related kinases like c-Met, Tie-2 and Aurora family.



**58:** R=cyclopropyl

**59:** R=H

**Figure 32.** Structural representation of **58** and **59**.

Sun *et al.* designed a series of compounds replacing diarylurea moiety with diaryl thiourea derivatives as dual EGFR and VEGFR-2 inhibitors (95). In these 6,7-dimethoxy quinazoline derivatives, it was observed that electron-donating groups on the terminal phenyl ring evidently decreased the activity. However, the placement of electron-withdrawing groups in the *meta* and *para* positions of the thiourea moiety enhanced the enzymatic activity. Altogether, an Oxygen atom as an ether linkage between the quinazoline core and diaryl thiourea group displayed less

enzymatic affinity than a thioether linker. Compounds **60** and **61** (Fig. 33) with significant EGFR and VEGFR-2 inhibitory activities ( $IC_{50}$  values for EGFR 0.02 and 0.01  $\mu$ M,  $IC_{50}$  values for VEGFR-2, 0.05 and 0.08  $\mu$ M respectively) also displayed superior antiproliferative activities against MCF-7, HT116 and B16 (murine melanoma cell line) than sorafenib (**Table 14**). These compounds were also tested for their in vivo antitumour activity against C57BL/6J mice carrying B16 tumour xenografts by oral administration at 90 mg/kg dosage, revealing that the tumour size reduction rate was higher than that of sorafenib. Molecular docking study of compound **61** (PDB code 4ASD) showed strong interactions between NH of thiourea group and Asp800 and methoxy group oxygen with Lys745.

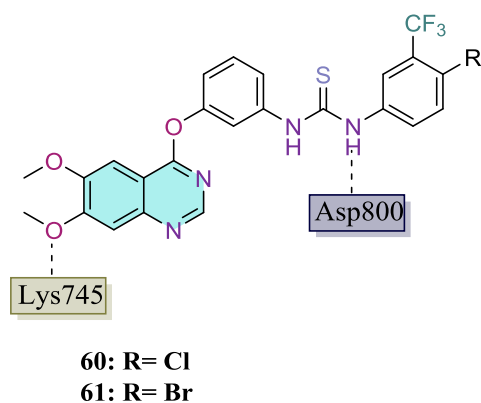


**Figure 33.** Structures of compounds **60** and **61**, binding mode of **61** into VEGFR-2 active site.

**Table 14**

Results of cellular evaluations of compounds **60** and **61**(data extracted from (95)).

Compounds	Effect on Cell Viability ( $EC_{50}$ , $\mu$ M)		
	HCT-166	MCF-7	B16
<b>60</b>	9.13	17.72	6.11
<b>61</b>	8.35	15.66	5.57
Sorafenib	10.55	17.87	9.29

Hamdi and colleagues introduced 4-anilino-2-vinylquinazoline derivatives as antitumour agents (96). SAR elucidation indicated that compounds containing the thiourea fragment and 4-bromostyryl at the C-2 position of the quinazoline core exhibited the best antiproliferative activity. Compound **65** (Fig. 34), with the highest cellular activity, inhibited the growth of HCT-166, Hep-G2 and MCF-7 cell lines with  $IC_{50}$  values of 8.62, 10.18 and 4.92  $\mu$ M accompanied by acceptable selectivity towards WI-38 normal human fetal lung fibroblast cell line. Moreover, **65** inhibited VEGFR-2 with an  $IC_{50}$  value of 60.27 nM, comparable to positive control, sorafenib ( $IC_{50}$  = 55.43 nM). Furthermore, **65** induced apoptosis more than sorafenib in

MCF-7 cancer cells and the cell cycle arrest into the G1/S phase. Compound **65** was well aligned in the binding mode of sorafenib (PDB code 4ASD) with key interactions between thiourea moiety, Glu885 and Asp1046 residue.

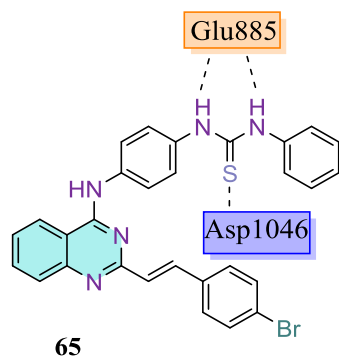


**Figure 34.** Structural representation and binding mode of **65** into VEGFR-2 active site.

Farouk *et al.* designed and synthesized five series of 6-bromo-2-(pyridin-3-yl) quinazoline-based compounds as multi tyrosine kinase inhibitors (97). Compounds containing various substituents at the C-4 position, such as phenyl urea, thiourea or isatin moieties were evaluated for their activity through VEGFR-2 inhibition. Compound **66** (Fig. 35) with a cyclohexyl thiourea fragment was found to be the most potent against VEGFR-2 with an  $IC_{50}$  value of 50.22 nM relative to the reference drug sorafenib ( $IC_{50} = 51.87$  nM). In addition, **66** was more effective than sorafenib against Hep-G2 and HCT-116 cells, with an acceptable selectivity toward WISH normal human fibroblast cell line as shown in **Table 15**. Cell cycle analysis and apoptosis of compound **66** were also studied in the HCT166 cell line; results show cell cycle arrest was mildly caused at the G1 phase also, the total apoptotic and necrotic cells percentage was increased after treatment with **66**. Additionally, based on the role of VEGF as an angiogenesis inductor, wound healing assay revealed a good inhibitory effect on HUVECs migration in addition to reduced closure percentage of induced wounds (51.111 %) compared to negative control with 97.037% closure. Docking studies (PDB code 4ASD) were conducted to find the binding pattern of **66**, in which two hydrogen bonds were observed between thiourea moiety and Glu885 and Asp1046, and another between nitrogen of pyridine and Cys919.

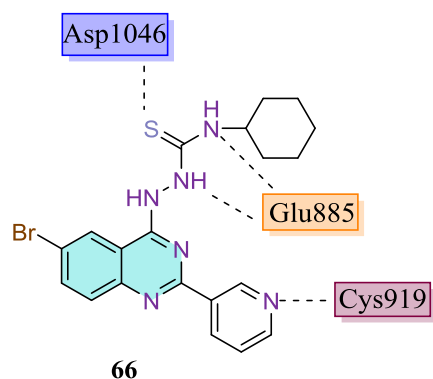


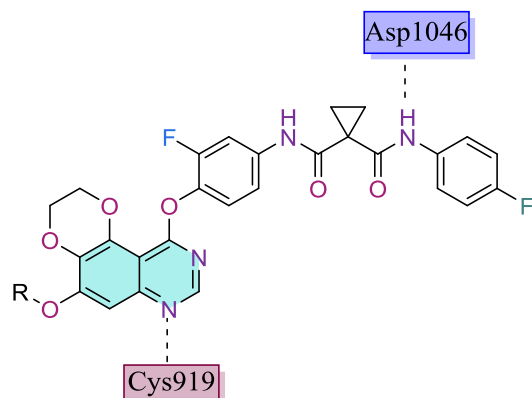
**Figure 35.** Structural representation and binding mode of **66** into VEGFR-2 active site.

**Table 15**

Results of cellular evaluations of compound **66** (data extracted from (97)).

Compound	Effect on cell viability (EC <sub>50</sub> , μM)		
	Hep-G2	HCT-116	WISH
<b>66</b>	10.40	3.37	49.59
Sorafenib	19.33	6.82	17.54

In another study, dual c-Met and VEGFR-2 inhibitors were designed by hybridizing [1,4]dioxino[2,3-f]quinazoline core with cyclopropane-1,1-dicarboxamide moiety present in cabozantinib (**98**). The placement of a small electron-withdrawing substituent at the *para* position of the terminal phenyl ring significantly enhanced the activity in contrast to the *meta* substituents. Also, positioning a Fluorine atom at C-2' and a methoxy ethyl group at the C-7 position of the quinazoline ring increased the activity. Compounds **67** and **68** (Fig. 36) were the two most potent compounds in enzymatic assays with IC<sub>50</sub> values of 4.8 and 3.5 nM against VEGFR-2, and against c-Met with 5.8 and 7.3 nM, respectively. Besides, they were active against liver cancer MHCC97H (human hepatocellular carcinoma cells) and V-HUVEC cell lines, as shown in Table 10. To evaluate the toxicity, the activity was tested against HEK293 and LO2 normal cell lines revealing favourable selectivity (**Table 16**). **67** was also tested against the MHCC97H xenograft mouse model, significantly inhibiting tumour growth (TGI = 120.4%) with almost no body weight change after 60 mg/kg PO administration, 4 times a day for 8 days. Docking of compound **67** into the ATP-binding site of VEGFR-2 (PDB code 3U6J) revealed that the NH of amide moiety forms a hydrogen bond with Asp1046, in addition to another hydrogen bond between N-1 of the quinazoline and Cys919.



**67:** R= 2-methoxyethyl

**68:** R= methyl

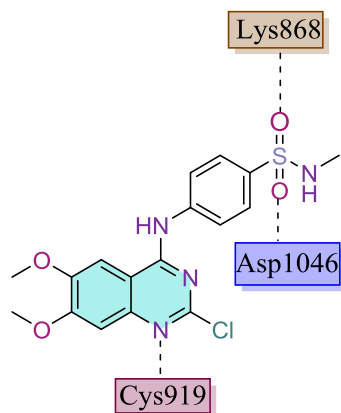
**Figure 36.** Structural representation of **67** and **68**, binding mode of **67** into VEGFR-2 active site.

**Table 16**

Results of cellular evaluations of compounds **67** and **68** (data extracted from (98)).

Compounds	Effect on Cell Viability (EC <sub>50</sub> , μg/mL)			
	MHCC97H (nM)	HUVEC (nM)	HEK293 (μM)	LO2 (μM)
<b>67</b>	15.1	12.6	11.9	12.2
<b>68</b>	58.6	3.7	15.1	12.6
Cabozantinib	25.0	2.7	-	-

Barbosa et al. reported a series of 4-anilinoquinazoline derivatives containing a Chlorine atom at the C-2 position as dual VEGFR-2 and EGFR inhibitors (99). The study revealed the importance of hydrogen bond donors by inserting sulfonamide and amide at the *para* position of the aniline ring. Additionally, replacing the methoxy groups at C-6 and C-7 with a hydrogen or methylenedioxy group dramatically decreased the activity. Among them, compound **69** (Fig. 37) had the highest VEGFR-2 inhibition with an IC<sub>50</sub> value of 0.85 μM, and also could inhibit EGFR<sub>wt</sub> equipotently (IC<sub>50</sub> = 1.63 μM). Docking studies of **69** (PDB code 4ASE) revealed a hydrogen bond between N-1 of the quinazoline core with Cys919 and the interaction of sulfone group as a hydrogen acceptor with Lys868 and Asp1046 residues.



69

**Figure 37.** Structural representation and binding mode of **69** into VEGFR-2 active site.

#### Equipment of HB donor/acceptor groups at C-4 position linked by an aliphatic chain

Sun *et al.* introduced two series of 4-benzyloxy quinazoline derivatives, one bearing a nitro group at the C-6 position as multi-kinase inhibitors (100). All compounds exhibited  $IC_{50}$  values less than 100 nM, selective against VEGFR-2. In general, this series of compounds exhibited superior enzymatic activity compared to their counterparts. Installation of a nitro group at the *para* position of the terminal benzyl ring compared to other substituents like halogens led to better enzymatic activity, like compound **70** (Fig. 38) with an  $IC_{50}$  value of 4.71 nM against VEGFR-2. Based on the above-mentioned information, a nitro-containing fragment (metronidazole) was replaced at the C-4 position of the quinazoline core. Surprisingly, cytotoxic activities were escalated, representing compound **71** (Fig. 38) as the inhibitor of VEGFR-2 with an  $IC_{50}$  value of 2.72 nM compared to EGFR, PDGFR and bFGF. **70** and **71** represented sub-micromolar  $IC_{50}$  values on A549, MCF-7 and H460 cell lines accompanied by remarkable selectivity against human macrophage cell line measured by CCK8 assay (**Table 17**). Treatment of **71** on the H460 cell line elevated the percentage of apoptotic cells in a dose-dependent manner after 48h. Molecular docking studies of compound **71** (PDB code 4ASE) showed a vital interaction between N-1 of quinazoline nucleus and Cys919 alongside with another bond between the nitro group at the 5 position of the imidazole ring with Asp1046.



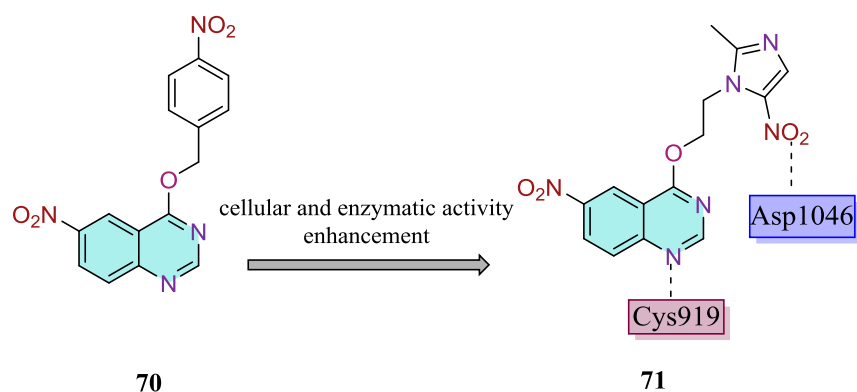


**Figure 38.** Structural representation of **70** and **71**, binding mode of **71** into VEGFR-2 active site.

**Table 17**

Results of cellular evaluations of compounds **70** and **71**(data extracted from (100)).

Effect on Cell Viability (EC <sub>50</sub> , μM)				
Compound	A549	MCF-7	H460	Macrophage
<b>71</b>	1.52	1.61	1.23	289.73
<b>72</b>	0.58	0.35	0.39	288.28
Tivozanib	0.62	0.38	0.39	226.75

Qiao and colleagues designed and synthesized a novel scaffold containing oxy methyl 1,3,4-oxadiazole at C-4 position of the quinazoline ring (101). Two separate series containing phenyl or benzyl moieties at 2 position of the oxadiazole ring were synthesized. Overall, compounds bearing the benzyl group exhibited superior cellular activity against MCF-7, A549 and Hela (Human cervical cancer cells) cell lines than the phenyl ring. All synthesized compounds showed selective inhibitory activity for VEGFR2 than for EGFR, bFGF and PDGFR. Positioning different substituents led to the understanding that the methoxy group and, after that halogen atoms (Br, Cl and F, respectively) in the order of *para* > *meta* > *ortho* increased the antiproliferative activity. SAR analysis resulted in compound **72** (Fig. 39) with 3,4-dimethoxy substituents revealing the best cellular activity with an IC<sub>50</sub> value of 0.23 against MCF-7 cell line superior to the positive control tivozanib. In addition, **72** showed the best VEGFR-2 inhibitory activity with an IC<sub>50</sub> value of 2.32 nM. The visual simulation of compound **72** (PDB code 4ASE) showed the formation of two hydrogen bonds, one between methoxy oxygen and Cys919 and one between oxygen atom linked to C-4 of quinazoline core and Asp1046, suggesting a higher binding affinity than tivozanib.

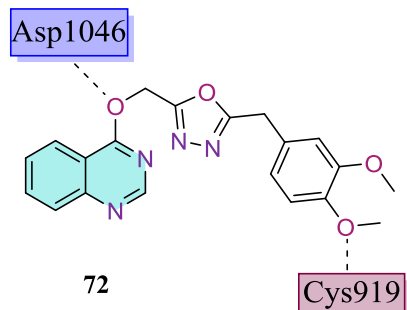


**Figure 39.** Structural representation and binding mode of **72** into VEGFR-2 active site.

Yin *et al.* reported a series of 4-oxoquinazoline derivatives linked by 2-propanol to various amine moieties at the C-4 position as potent VEGFR-2 inhibitors (102). Compounds containing piperazine fragments represented favorable cytotoxic activities; among them, compounds with aromatic moieties linked to piperazine were the most potent. Insertion of different substituents at the terminal phenyl ring revealed that the methoxy group exhibited superior cytotoxic activity. Compound **73** (Fig. 40), with the highest VEGFR-2 inhibition, elicited an  $IC_{50}$  value of 2.89 nM, better than tivozanib ( $IC_{50} = 3.38$  nM), alongside an acceptable selectivity against EGFR, bFGF and PDGFR. **73** exhibited  $IC_{50}$  values in the sub-micromolar range against MCF-7, A549 and HeLa cell lines, and with remarkable selectivity against human macrophage cells. **73** also triggered apoptosis in MCF-7 cells in a dose-dependent manner. Although, in visual inspection of compound **73** it was clearly seen that it had obviously lower interaction energy than tivozanib.

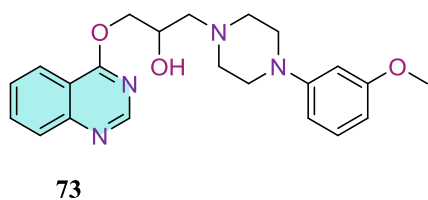


**Figure 40.** Structural representation of **73**.

### Equipment of HB donor/acceptor groups at C-5 position

Xi *et al.* introduced 4-hydroxy-8-nitro-5-substituted quinazolines as VEGFR-2 inhibitors (103). Installation of aliphatic or aromatic diamines at C-5 of the quinazoline ring led to compounds with different activity profiles. Aside from 1,4-dianiline substituents that were significantly

active against VEGFR-2, the aliphatic diamines or the other aromatic dianiline substitutions (1,3-dianiline and 1,2-dianiline) had  $IC_{50}$  values over 10  $\mu$ M. Also, substituting electron-withdrawing groups on the terminal phenyl ring escalated the enzymatic activity. For instance, compound **74** (Fig. 41) bearing 2-Cl-5-CF<sub>3</sub>C<sub>6</sub>H<sub>3</sub> moiety manifested the best VEGFR-2 activity with an  $IC_{50}$  value of 12 nM. Presumably, none of the compounds had any enzymatic activity against EGFR. Nearly all the synthesized compounds did not show antiproliferative activity against HUVEC, Hep-G2, MCF-7 and SK-OV-3 (human ovarian cancer cells) cell lines, although a number of them represented weak activity, like **74**. According to the authors, this may be caused by ionization of the C-4 OH group, causing a decrease in log D, thus lowering membrane permeability. Visual simulation of **74** (PDB code 1YWN) showed hydrogen bond formation between OH group at C-4 of quinazoline and Cysteine residue in hinge region, along with the interaction of urea moiety with the active aspartic acid and glutamic acid residues in the active site.

In an attempt to enhance the antiproliferative activity of compound **74**, Zhao et al. replaced the urea moiety with an amide group to develop new arylamide-5-anilinoquinazoline-8-nitro derivatives (104). SAR analysis was in agreement with the previous study, confirming that linear aryl 1,4-diamine linker was more active than aryl 1,3-diamine homologues. Likewise, electron-withdrawing groups at the *para* position of the terminal phenyl ring could improve the inhibitory activity. According to enzymatic assay results, all compounds displayed selectivity against VEGFR-2 than EGFR; consequently, all compounds were more potent against VEGFR-2 dependent cell lines HUVEC and Hep-G2 compared to A549 and MDA-MB-231 (human breast cancer cells) cell lines. Compound **75** (Fig. 41), with the best VEGFR-2 inhibition ( $IC_{50}$  = 64.9 nM), also exhibited the best cellular inhibition profile as shown in **Table 18**. Exploring angiogenesis in CAM assay revealed that **75** had better anti-angiogenic activity than sorafenib. Additionally, **75** increased the apoptotic ratio in Hep-G2 cells from 2.6 % to 72.2% (at 10 nM concentration after 24 h) compared to the blank control. Moreover, an increased percentage of cells in the G<sub>0</sub>/G<sub>1</sub> phase was shown by the cell cycle analysis of **75** in a concentration-dependent manner. Docking studies supported the binding mode of **75** (PDB code 3WZE) in the manner of three hydrogen bonds between nitro group and two nitrogen atoms of the quinazoline core with Cys919, NH of the amide moiety with Glu885, and the carbonyl of the amide with both Cys1045 and Asp1046 residues.

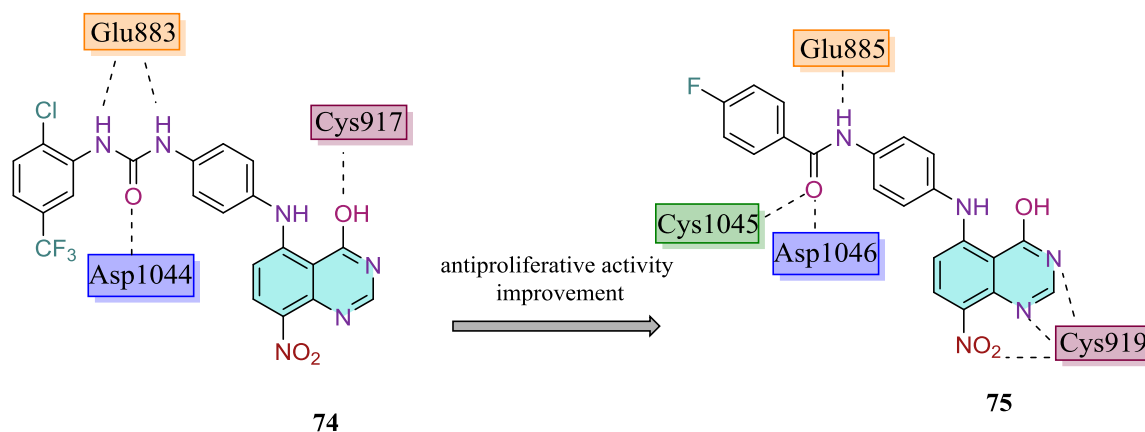


**Figure 41.** Structural representation and binding modes of **74** and **75** into VEGFR-2 active site.

**Table 18**

Results of cellular evaluations of compound **75** (data extracted from (104)).

Compounds	Effect on Cell Viability (EC <sub>50</sub> , μM)			
	HUVEC	Hep-G2	A549	MDA-MB-231
<b>75</b>	0.5	0.2	69	58.4
Sorafenib	4.1	3.6	8.1	15.8
Ponatinib	0.5	0.6	5.3	10.5

### Equipment of HB donor/acceptor groups at C-7 position

Zhang *et al.* reported a series of 2-aminoquinazoline bearing diaryl thiourea moiety at the C-7 position as multi-kinase inhibitors (105). Among synthesized compounds, those containing trifluoromethyl or trifluoromethoxyl displayed promising activities. The best enzymatic profile was observed in compound **76** (Fig. 42) against angiogenesis-related enzymes, VEGFR-2, Tie-2 and EphB4, as shown in **Table 19**. Further assessments of **76** on Ea.HY926 (human vascular endothelial cells) cell line revealed an IC<sub>50</sub> value of 7.56 μM. Moreover, molecular docking studies **76** in the VEGFR-2 active site showed the formation of two hydrogen bonds between nitrogen atoms of thiourea fragment with Asp1046 residue.

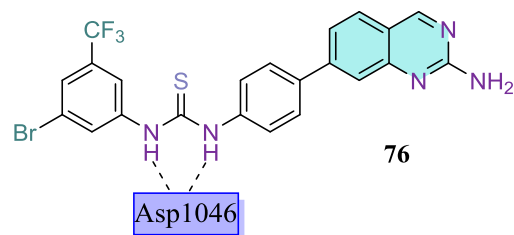


**Figure 42.** Structural representation and binding mode of **76** into VEGFR-2 active site.

**Table 19**

Results of enzymatic evaluations of compounds **76** (data extracted from (105)).

Inhibition Level (IC <sub>50</sub> , nM)			
Compound	VEGFR-2	TIE-2	EphB4
<b>76</b>	1.05	2.47	0.27
Sorafenib	0.45	0.83	0.20

Zhang *et al.* designed and synthesized a series of quinazolin-4(3*H*)-one containing diaryl urea substituents at the C-7 position as anti-angiogenic agents (106). Compound **77** (Fig. 43) showed the best enzymatic activity, particularly against VEGFR-2, with an IC<sub>50</sub> value of 0.77 nM compared to that of sorafenib (IC<sub>50</sub> = 0.55 nM). Enzymatic activity on angiogenesis-related kinases and the selectivity profile of **77** is shown in detail in **Table 20**. The best antiproliferative activity was also observed by **77** on EA.hy926 cells with an IC<sub>50</sub> value of 2.69 μM. Further assessments on **77** against a panel on cancer cell line revealed acceptable activity accompanied with good selectivity against QSG7701 (human hepatocyte cell line) and HEK293 normal cell lines (**Table 21**). Compound **77** induced early apoptosis on EA.hy926 treated cell line in a dose-dependent manner. Furthermore, screening of **77** on MCF-7 xenograft mice model with maximum tested dose (80 mg/kg) inhibited tumour growth by 47%, which was less than that of sorafenib, revealing 53% TGI at 40 mg/kg dosage. Docking studies on **77** showed that quinazolin-4(3*H*)-one core occupies the hinge region of the VEGFR-2 active site.

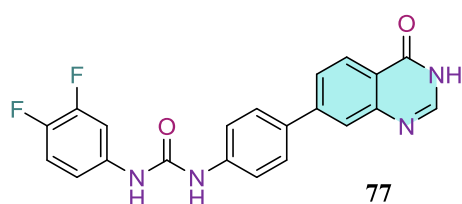


**Figure 43.** Structural representation of **77**.

**Table 20**

Results of enzymatic evaluations of compounds **77** (data extracted from (106)).

Compounds	Inhibition Level (IC <sub>50</sub> , nM)									
	VEGFR-2	Tie-2	EphB4	VEGFR-1	EGFR	PDGFR-β	c-Kit	FGFR-1	FGFR-4	B-Raf

<b>77</b>	0.77	8.87	3.21	192	98.8	98.5	142	176.2	>500	>500
Sorafenib	0.55	4.65	3.00	-	-	-	-	-	-	-

**Table 21**

Results of cellular evaluations of compounds **77** (data extracted from (106)).

Compound	Effect on Cell Viability (EC <sub>50</sub> , μM)							
	EA.hy926	SMMC-7721	MCF-7	PANC-1	A431	A549	LOVO	HeLa
<b>77</b>	2.69	58.7	2.12	24.9	16.9	8.37	4.99	5.56

Yang et al. introduced novel 4-anilinoquinazoline compounds bearing urea moiety at the C-7 position by hybridizing the structures of gefitinib and sorafenib as dual EGFR/VEGFR-2 inhibitors (107). Best antiproliferative activities were observed in cases of small alkyl groups on the C-4' position and 3-CF<sub>3</sub> and 4-Cl substituents on the phenyl ring linked to the urea group. Compound **78** (Fig. 44) showed the best cellular activity in A549, HT-29 and MCF-7 cell lines (IC<sub>50</sub>s 1.76, 0.81 and 2.49 μM, respectively) and also represented an IC<sub>50</sub> value of 2584 nM against VEGFR-2. Compound **79** (Fig. 44), with the best VEGFR-2 inhibitory activity (IC<sub>50</sub> = 479 nM) showed poor activity against the three mentioned cell lines. Further assessment also revealed that **78** could induce apoptosis in the A549 cell line compared to the negative control.

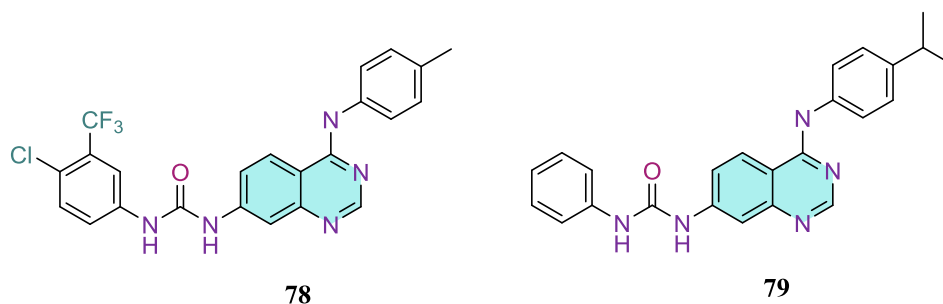


**Figure 44.** Structural representation of **78** and **79**.

### Equipment of HB donor/acceptor groups at C-2 or N-3 positions

Patel *et al.* gathered a series of quinazoline-based VEGFR-2 inhibitors from the literature, passing them through different filters of virtual screening to achieve a pharmacophore-based 3D QSAR model (108). By utilizing this model, they synthesized a novel series of 6,7-dimethoxy-2-phenylquinazolin-4(3*H*)-one derivatives with various substituents at the N-3 position. Among them, thiadiazole-containing analogues were more potent compared to oxadiazole and aniline-

containing counterparts. Also, less bulky substituents at the C-5 position of the thiadiazole and oxadiazole reduced the activity. The presence of an electron-withdrawing group at the *para* position of the terminal phenyl ring dramatically enhanced the activity. Compounds elicited IC<sub>50</sub> values against VEGFR-2 ranging from 3.8 to 124 nM. The most potent compound **80** (Fig. 45), revealed the best inhibitory activity against HUVEC with an IC<sub>50</sub> value of 5.5 nM. Docking simulation revealed the formation of a hydrogen bond between N-1 of the quinazoline nucleus and the hydrogen atom of the Cys919 in the backbone of the ATP binding cavity of VEGFR-2.

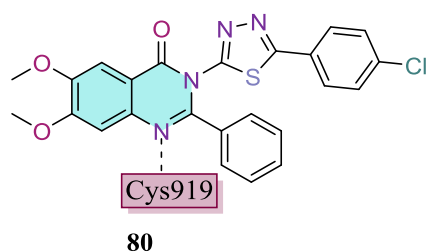


**Figure 45.** Structural representation and binding mode of **80**.

Since 2017 several research groups have introduced novel VEGFR-2 inhibitors by the placement of long side chains at C-2 or N-3 of the quinazoline core. As opposed to previous mentions where the quinazoline core was involved in an interaction with the hinge region, other hydrogen donor/acceptor moieties play a role in the formation of essential interactions in the hinge region at the active site of VEGFR-2.

Considering 4-oxobenzoquinonazolines with benzene sulfonamide at the N-3 position of the tricyclic ring as the main core, Ghorab et al. studied the effects of hydrazinyl or pyrazolyl derivatives at the C-2 position (109). Authors reported IC<sub>50</sub> values ranging from 0.10 to 26.65  $\mu$ M against MCF-7 cell line, with the most potent being compound **81** (Fig. 46) containing 2,4-dichlorobenzylidene hydrazinyl at the C-2 position. Also, compound **81** revealed the highest VEGFR-2 inhibition with an IC<sub>50</sub> value of 0.64  $\mu$ M. Docking stimulation elucidated cation- $\pi$  interaction was formed between two phenyl rings of the tricyclic ring supporting their pharmacophoric hypothesis. Further apoptosis studies were performed on **81**, evaluating activation of caspase-3 and effects on expression levels of Bcl-2 and Bax proteins compared to reference drug, vandetanib. Performing a flow cytometry assay on the MCF-7 cells treated with

**81** indicated that 24.17% of cells were arrested at the G2/M phase compared to 4.82% of untreated control found at the G2/M phase. **81** also showed a selective cytotoxic effect on normal cell line MCF-12A which was better than vandetanib.

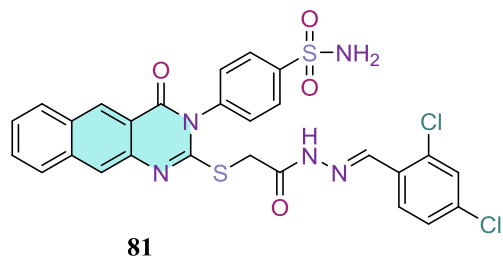


**Figure 46.** Structural representation and binding mode of **81** into VEGFR-2 active site.

Following the previous study, Soliman et al. continued working on similar structures for dual EGFR and VEGFR-2 inhibitory activity, with a 4-oxoquinonazolines core containing benzene sulfonamide at the N-3 position and different thioacetamide groups at the C-2 position of the quinazoline ring (110). Synthesized compounds screened for antiproliferative activity against the MDA-MB-231 breast cancer cell line displayed IC<sub>50</sub> values ranging from 0.34 to 149.10  $\mu$ M. The most potent compound against VEGFR-2 was 2,3-dimethoxy benzyl derivative **82** (Fig. 47), with an IC<sub>50</sub> value of 247.38 nM. The relative safety of **82** was also tested, displaying low toxicity against the MCF-10 normal human breast cell line. Furthermore, **82** sensitized gamma irradiated MDA-MB-231 cells to radiotherapy by decreasing IC<sub>50</sub> value from 1.91 to 0.51  $\mu$ M. Molecular docking of **82** in the active site of VEGFR-2 (PDB code 4AGD) showed two hydrogen bonds between NH of sulfonamide with Cys919 and the methoxy at the 2 position of the terminal phenyl ring with Asp1046.

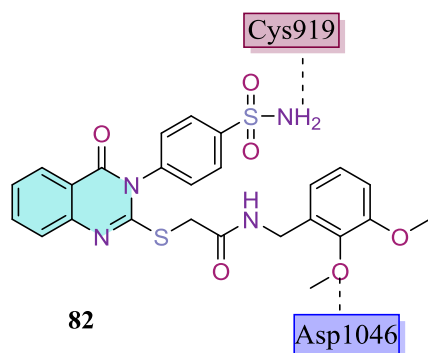




**Figure 47.** Structural representation and binding mode of **82** into VEGFR-2 active site.

Mahdy *et al.* reported a series of 4-oxoquinazoline compounds hybridized with essential pharmacophoric features at C-2 and N-3 positions based on documented and clinically approved VEGFR-2 inhibitors (111). Insertion of various alkyl and hetero alkyl long chains revealed that positioning derivatives at C-2 were tolerated better than N-3. Compound **83** (Fig. 48) exerted the best cellular activity profile against HepG-2, HCT-116 and MCF-7 cell lines with IC<sub>50</sub> values of 3.97, 4.83 and 4.58 μM, respectively. In terms of evaluating biochemical studies effects of **83** on enzymatic inhibition, cell cycle and induction of apoptosis were examined. **83**, which has an IC<sub>50</sub> value of 2.5 μM against VEGFR-2, arrested cell growth in the G2/M phase and induced apoptosis by more than 14-fold over the untreated Hep-G2 cells using Annexin V and PI double staining assay. In vivo anticancer activity was also evaluated using diethylnitrosamine (DEN)-induced hepatocellular carcinoma model. A photomicrograph of the liver for DEN-53 treated rats confirmed that **83** possessed significant tumour growth inhibition. Molecular docking of this compound into kinase domain (PDB code 2OH4) further revealed that the amide segment of **83** binds to key regions of VEGFR-2 active site with two hydrogen bonds.

In continuation of previous work, Eissa et al. altered **83** by replacing the phenyl ring instead of the ethyl group at N-3 position, assuming that it will boost binding affinity by increasing interaction with the allosteric hydrophobic back pocket of VEGFR-2 (112). Modifications resulted in compound **84** (Fig. 48) with a 2-hydroxyl phenyl group linked to hydrazone moiety, which exhibited the highest cellular activity. IC<sub>50</sub> values of **84** against HepG-2, HCT-116 and MCF-7 were 3.74, 5.00 and 6.77 μM, respectively, which was better than those of reference drugs sorafenib and doxorubicin. Authors reported a range of 0.340 to 0.751 μM for VEGFR-2 inhibition for selected compounds, the most potent being **84**. Compound **84** satisfied the hot spots, where the hydrogen bonds between NH of hydrazino and the terminal OH group were observed with key residues of VEGFR-2 active site.

Continuing the previous study, El-Adl *et al.* inserted a p-tolyl group replacing the phenyl ring at the N-3 of the quinazoline scaffold (113). This adjustment led to **85** (Fig. 48) containing a 2-chloro-5-nitrophenyl moiety as a terminal hydrophobic moiety, which had superior cytotoxic activities. **85** had IC<sub>50</sub> values of 1.88, 1.68 and 3.91 μM against Hep-G2, HCT-116 and MCF-7 cell lines, respectively. Inspection of enzymatic activity revealed an IC<sub>50</sub> value of 0.290 μg/ml

versus VEGFR-2, greater than that of sorafenib ( $IC_{50} = 0.588 \mu\text{g/ml}$ ). Molecular docking of **85** showed that NH of hydrazone moiety and the carbonyl oxygen adjacent to it form key hydrogen bonds with VEGFR-2 active site, additionally, carbonyl group at C-4 of quinazoline core interacts with Asn921 residue.

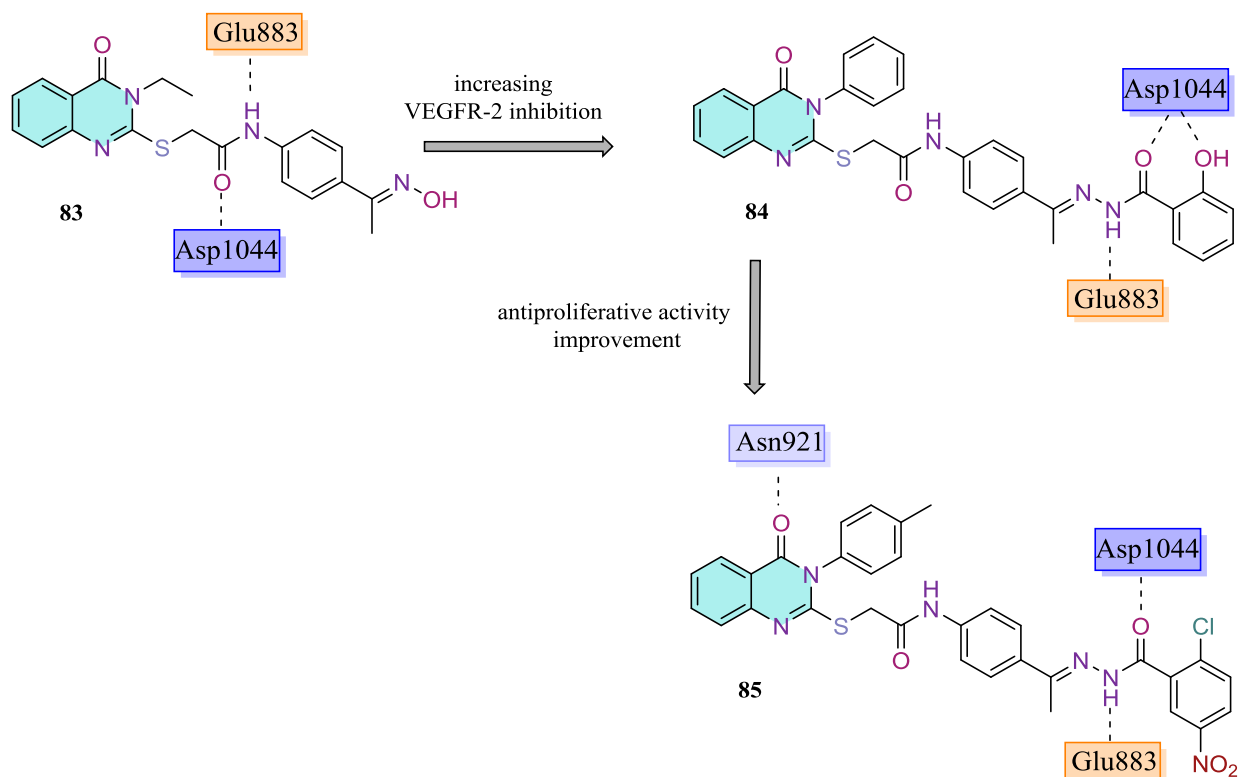


**Figure 48.** Structural representation and binding modes of **83-85** into VEGFR-2 active site.

El-Adl *et al.* reported a series of 1-benzylquinazoline-2,4(1H,3H)-dione derivatives as VEGFR-2 inhibitors (114). Compounds containing hydrazone linker in the long side chain connected to the N-3 position exhibited the best cytotoxic activities. In this series, substitution on the terminal phenyl moiety led to compounds with better activities than the unsubstituted counterparts. Compound **86** (Fig. 49), as the most potent agent, exhibited  $GI_{50}$ s of 9.16, 5.69 and 5.27  $\mu\text{M}$  against Hep-G2, HCT-116 and MCF-7 cell lines, respectively. **86** had an enzymatic activity with an  $IC_{50}$  value of 0.12  $\mu\text{M}$  against VEGFR-2, which was higher than the reference drug sorafenib ( $IC_{50} = 0.1 \mu\text{M}$ ). Docking studies (PDB code 2OH4) revealed that compound **86** has hydrogen bond interactions between both carbonyl group of acetamide linker and carbonyl group at C-4 of quinazoline core with aspart residue of DGF-motif in the binding cavity of

VEGFR-2. This binding model was in complete agreement with what had been observed for sorafenib as a type II inhibitor.

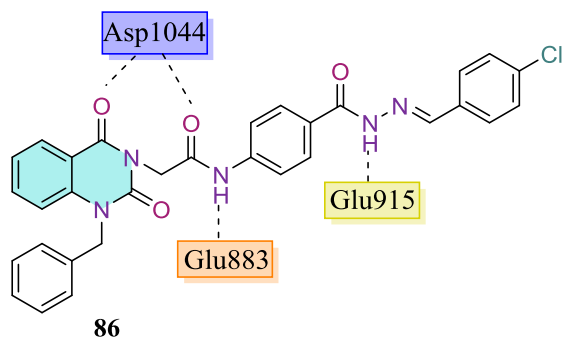


**Figure 49.** Structural representation and binding mode of **86** into VEGFR-2 active site.

Zahran et al. designed and synthesized quinazolinone-based compounds containing the sulfachloropyridazine moiety at C-2 or N-3 positions (115). NCI-60 panel was used to screen all compounds against various cancer cell lines. All compounds had an average growth inhibition percentage of less than 10  $\mu$ M. Among the more active compounds in cellular inhibition, compound **87** (Fig. 50) was the most active against VEGFR-2 with an  $IC_{50}$  value of 66 nM. Additionally, compound **87** showed moderate inhibition against PDGFR, EGFR, and FGFR-1 ( $IC_{50}$ = 180, 98 and 82 nM, respectively), as well as the ability to reduce cell migration in wound healing assays. Cell cycle control was interfered by compound **87**, resulting in cell cycle arrest into the S phase and apoptosis at both early and late stages in UO-31 human renal cancer cells. In addition, compound **87** elevated the level of caspase-3 and upregulated Bax expression and downregulated Bcl-2 in UO-31 cells. Also, compound **87** showed low toxicity against the human normal renal (RPTEC) cell line. Assessment of the binding mode of compound **87** by docking studies (PDB code 4ASD) elucidated one hydrogen bond between pyridazine motif and Cys919, and two others between the acetamide group with Glu885 and Asp1046 residues.

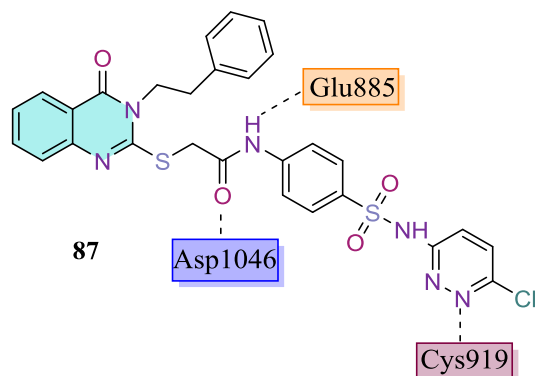


**Figure 50.** Structural representation and binding mode of **87** into VEGFR-2 active site.

Fusion of quinazoline ring with other heteroarmatic moieties has been a novel strategy in kinase inhibition (116, 117). Based on this strategy, Azab *et al.* designed a series of [1,2,4]triazolo[4,3- c]quinazoline derivatives as VEGFR-2 inhibitors (118). Various substituents were placed on the terminal hydrophobic moiety and results showed that the best activity was observed in *ortho*-chloro substituted compounds. The most promising antiproliferative agent was compound **88** (Fig. 52), with an IC<sub>50</sub> value of 4.88 and 5.21 μM against Hep-G2 and HCT-116, respectively. Additionally, the best enzymatic activity was observed in compound **88**, with an IC<sub>50</sub> value of 53.81 nM against VEGFR-2 comparable with sorafenib (IC<sub>50</sub> = 44.34 nM). Cell cycle analysis resulted in arrest in both S and G2/M phases on Hep-G2 cells. Compound **88** produced more than 10-fold increase in apoptotic cells in the early phase compared to the negative control. **88** also increased the level of caspase-3 expression and upregulated Bax and downregulated Bcl-2 expression in Hep-G2 cells. Inspection of docking results of compound **88** occupying the VEGFR-2 active site (PDB code 2OH4) revealed vital interactions between hydrazide moiety and DFG-motif, also between triazole moiety and cysteine residue of the hinge region.

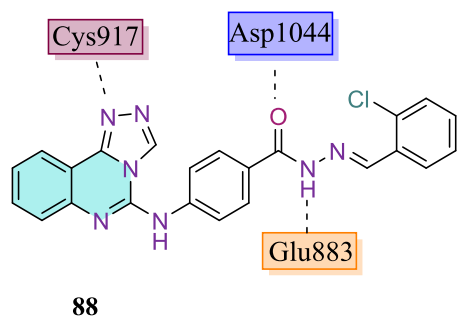


**Figure 52.** Structural representation and binding mode of **88** into VEGFR-2 active site.

E. Abdallah *et al.* reported a series of quinazolin-4(3*H*)-one derivatives as VEGFR-2 inhibitors (119). All compounds were tested against the VEGFR-2 enzyme; among them, only compound **89** (Fig. 53), with a nitro group at the C-6 position, revealed higher activity (IC<sub>50</sub>= 4.6 μM) than the reference drug, pazopanib (IC<sub>50</sub>= 4.8 μM). Compounds with better enzymatic activities were tested against cancerous cell lines Hep-G2, PC3 and MCF-7 as well as the WI-38 normal cell line, revealing that **89** also had the best antiproliferative activity accompanied with a good selectivity profile (**Table 22**). Cell cycle analysis showed an arrest on the G2/M phase on

Hep-G2 cells treated with **89**. Also, the percentage of apoptosis was increased from 2.37% to 18.33% compared to the negative control. Molecular docking simulation of compound **89** (PDB code 3VHE), showed a vital interaction between nitro group and Cys919, and also two hydrogen bonds between oxohydrazone moiety, Glu885 and Asp1046 residues.

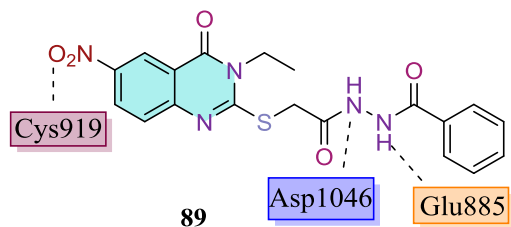


**Figure 53.** Structural representation and binding mode of **89** into VEGFR-2 active site.

**Table 22**

Results of cellular evaluations of compounds **89** (data extracted from (119)).

Compound	Effect on Cell Viability (EC <sub>50</sub> , µg/mL)			
	Hep-G2	PC3	MCF-7	WI-38
<b>89</b>	17.23	26.10	30.85	145.93
Doxorubicin	7.94	8.87	6.75	ND

Ahmed *et al.* synthesized various quinazoline derivatives bearing thio acetohydrazone moiety as VEGFR-2 inhibitors (120). Compound **90** (Fig. 54) was reported as the most potent antiproliferative agent with IC<sub>50</sub> values of 9.63 and 1.58 µM versus MCF-7 and HCT-116 cell lines accompanied by an IC<sub>50</sub> value of 3.19 µM against VEGFR-2 comparable to positive control sorafenib (IC<sub>50</sub> = 3.24 µM). Compound **90** interrupts the cell cycle of HCT-116 cells in the G2/M phase and triggers apoptosis by raising caspase-3, Bax and p53 levels alongside with alleviation of Bcl-2 level.

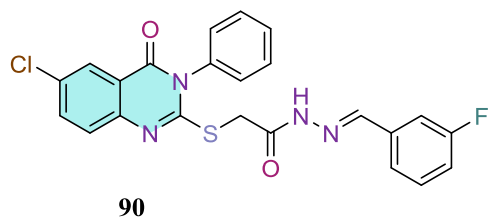


**Figure 54.** Structural representation of **90**.

Eissa *et al.* designed a series of quinazolin-4(3H)-ones as VEGFR-2 inhibitors (121). The presence of an extended side chain containing a linker (NH, acetamide or thioacetamide) and a hydrogen bond acceptor/donor groups connected to the terminal hydrophobic moieties were examined at C-2 or N-3 positions. According to their SAR analysis, authors reported that the

placement of elongated substituents at the C-2 position was preferred to N-3. For hydrogen-bond donors/acceptors, sulfonylthiourea group exhibited better activity than sulfonamide moiety. Additionally, ethyl group attached to N-3 was more advantageous than the phenyl moiety. Accordingly, compound **91** (Fig. 55) possessed the best cellular activity against Hep-G2 with an  $IC_{50}$  value of 4.33  $\mu\text{g/ml}$  and an  $IC_{50}$  value of 3.1  $\mu\text{M}$  versus VEGFR-2, comparable to sorafenib ( $IC_{50} = 2.4 \mu\text{M}$ ). Compound **91** could induce both early and late cellular apoptosis in Hep-G2 cell line. *In vivo* treatment of rats in (DEN)-induced hepatocellular carcinoma by compound **91** improved histological features of the liver, revealing the tumour growth inhibition. Exposure of compound **91** to Hep-G2 cells increased cleaved caspase-3 protein expression in a time-dependent manner. Furthermore, **91** possessed a fibro-protective effect and could attenuate liver fibrosis in the fibroblastic proliferative index test. Inspection of molecular docking of the target compound, (PDB code 2OH4) revealed the formation of two hydrogen bonds between the sulfonylthiourea moiety and the DFG-motif of VEGFR-2 active site.

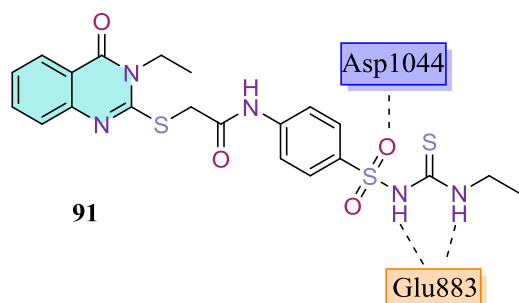


**Figure 55.** Structural representation and binding mode of **91** into VEGFR-2 active site.

A. Abuelizz and colleagues reported a series of 4-oxobenzoquinazoline derivatives with different substituents at C-2 and N-3 positions for anticancer activity (122). Among them, compound **92** (Fig. 56), with the highest VEGFR-2 inhibition ( $IC_{50} = 44.4 \text{ nM}$ ), presented  $IC_{50}$  values of 26.0 and 9.4  $\mu\text{M}$  versus Hep-G2 and MCF-7 cell lines, respectively. Compound **92**, as a type II inhibitor, had vital interaction between N1 of the quinazoline core with Asp1046 and oxygen of the isoindoline moiety with Cys919 in the hinge region (PDB code 4ASE).

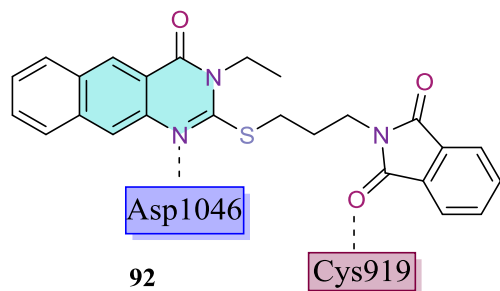


**Figure 56.** Structural representation and binding mode of **92** into VEGFR-2 active site.

### Irreversible inhibitors

A great deal of effort has been put into designing small molecules that can irreversibly inhibit kinase protein family members. Until now, different drugs such as neratinib and dacomitinib, targeting EGFR kinase, and ibrutinib, zanubrutinib and tinabrutinib, targeting BTK kinase, have been approved by FDA for various types of cancer, while an approved irreversible VEGFR-2 inhibitor has not been reported yet. Studies by Wissner *et al.* evaluated the possibility of irreversible VEGFR-2 inhibition.

Investigation on the binding model of compound **2** (Fig. 7) at the active site of VEGFR-2 revealed that Cys-1045 residue was located near the 4-anilino group of compound **2**. A new series of quinazoline-based compound, as a covalent inhibitor of VEGFR-2, might be possibly obtained by substitution of the 4-anilino group at this core with a reactive group at the same size, quinone ring (123). Assumingly, the quinone moiety acts as an electrophile, and Cys-1045 acts as a nucleophile; the reactivity of this system could be calculated by determination of difference in energy levels of the HOMO of the nucleophile and the LUMO of the electrophile. Significant relativity was observed between calculated LUMO energies and the conformation of the inhibitors with respect to the variety of substituents of the quinone ring. It was concluded that LUMO of the compounds has a  $\pi$ -character, mainly centered on the quinone ring; thus, alkoxy and halogens containing derivatives at the 5 and/or 6 positions of the quinone ring decreased the LUMO energy making them more reactive. In contrast, electron-donating groups such as alkylamino substituents increase it, making them less reactive. At the 3-position of the quinone ring, the presence of any substituents interfered with the orientation to the quinazoline core,

alleviating the inhibitory activity. The side chains at the C-6 and C-7 positions of the quinazoline ring were also altered to improve the bioavailability. Apart from the target enzyme, it's evident that there are other nucleophilic species (like glutathione or other proteins) in the circulation or the cytosol; consequently, some of the more reactive quinone derivatives lost their activity in the presence of GSH and plasma. Among all synthesized compounds, **93** (Fig. 57) had the most interesting inhibitory profile with the  $IC_{50}$  value of 5.1 nM in the presence of 10  $\mu$ M ATP. Compound **93** demonstrated  $IC_{50}$  values of 6.9 and 3.7 nM in the presence of 100  $\mu$ M GSH and 5% plasma, respectively; this suggested that the significant portion of enzyme activity was retained in the presence of GSH and plasma. Comparison between  $IC_{50}$  values of **93** in the presence of 10  $\mu$ M ATP and 1 mM ATP (5.1 and 11.2 nM, respectively) indicates that compound **93** is a non-competitive ATP inhibitor. The reactivity of **93** was evaluated against a panel of other kinases, which showed 120-500 times more potency in inhibiting VEGFR-2 compared to LCK and PI3K. Compound **93** also showed a 54% reduction in the human colon carcinoma tumour mass after 20 days of exposure compared to the control animal group in the *in vivo* evaluation experiment.

Following the previous study, Wissner *et al.* designed a series of compounds using a quinazoline scaffold to form covalent interactions with Cys-773 in EGFR and Cys-1045 in VEGFR-2 to achieve dual irreversible inhibitory activities (124). Enzymatic assay examinations revealed that each compound having 4-(dimethylamino) crotonamide as a Michael acceptor group would be an EGFR inhibitor and each compound with quinone ring would be a VEGFR-2 inhibitor. Compounds containing both mentioned reactive groups inhibited these enzymes as non-ATP-competitive inhibitors.

Compound **94** (Fig. 57) showed the best VEGFR-2 inhibitory activity with  $IC_{50}$  values of 76.2 and 298.0 in the presence of 1  $\mu$ M and 1 mM ATP, respectively.



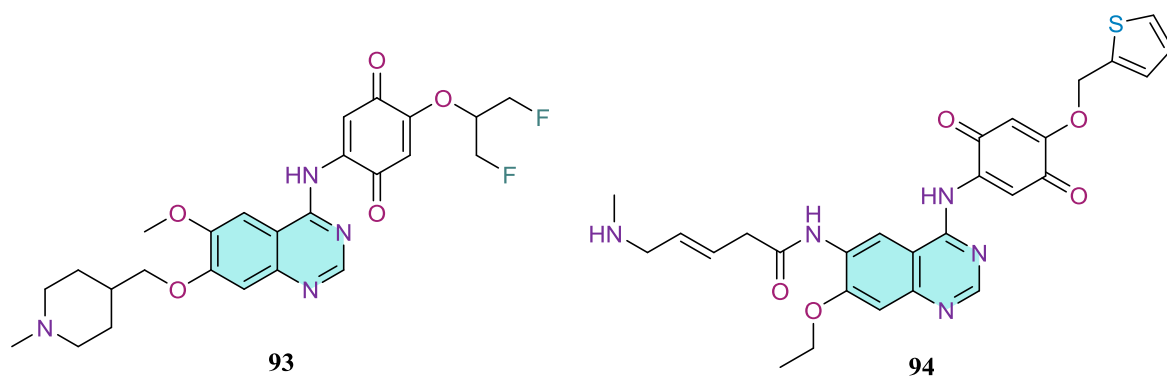


**Figure 57.** Structural representation of **93** and **94**.

## Conclusion

In recent years, targeted cancer therapy has been one of the fastest growing areas of research in chemotherapy thanks to high efficacy seeking and side effect minimization needs. Angiogenesis inhibition appears unique and promising for the suppression of tumours in various cancer types. Factually, anti-angiogenic agents block the growth of blood vessels that support tumour growth rather than blocking the cancerous cells themselves; therefore, these agents appear to have fewer common adverse effects compared to other chemotherapy agents. VEGFR-2 is the most studied kinase in anti-angiogenic drug discovery. In recent years, efforts have escalated significantly to focus on developing new VEGFR-2 inhibitors. As one of the first established scaffolds in the evolution of kinase inhibitors, quinazoline core is frequently used as an ATP mimetic with more than twenty approved drugs to this date. Despite the availability of various medications, there are still intrinsic and acquired resistances observed with available treatments. Therefore, there is an urgent need to introduce novel drugs for the improvement of clinical efficacy and safety profile of current medications. Here we have summarized the classic SAR analysis and biochemical properties of reported quinazoline-containing scaffolds. The main purpose of this review was to explore and highlight the importance of quinazoline derivatives in targeting VEGFR-2 as a critical strategy in cancer treatment. As a near future perspective, it is reasoned to believe that there are possibilities of utilizing VEGFR-2-PROTAC degraders (125) based on quinazoline core, since it has been reported in other types of kinases (126, 127, 128).

## **Declaration of competing interest**

The authors declare that they have no known competing financial interests or personal relationships that could have appeared to influence the work reported in this paper.

## **Acknowledgments**

We are very grateful to acknowledge financial support from Kerman Neuroscience Research Center, Kerman University of Medical Sciences.

Stéphane Bach thanks the Cancéropôle Grand Ouest (Network of Western France cancer centres, Appel d'Offres Structurant 2021, "RPM" CGO/ Conseil Régional de Bretagne) for supporting his work on the inhibition of cancer-related kinases.

Johanna Giovannini is supported by a CNRS France Relance grant (R&D program "CARACTHERA").

Also, special thanks to Touka Fatemi for her help with this work, also thanks to Dr. Mohammad Javad Dehghan for his kind supports.

## **References**

1. Shah AA, Kamal MA, Akhtar S. Tumor angiogenesis and VEGFR-2: mechanism, pathways and current biological therapeutic interventions. *Current Drug Metabolism*. 2021;22(1):50-9.
2. Risau W. Mechanisms of angiogenesis. *Nature*. 1997;386(6626):671-4.
3. Munoz-Chapuli R, Quesada A, Angel Medina M. Angiogenesis and signal transduction in endothelial cells. *Cellular and Molecular Life Sciences CMLS*. 2004;61:2224-43.
4. De Palma M, Biziato D, Petrova TV. Microenvironmental regulation of tumour angiogenesis. *Nature Reviews Cancer*. 2017;17(8):457-74.
5. Rege TA, Fears CY, Gladson CL. Endogenous inhibitors of angiogenesis in malignant gliomas: nature's antiangiogenic therapy. *Neuro-oncology*. 2005;7(2):106-21.
6. Yoo SY, Kwon SM. Angiogenesis and its therapeutic opportunities. *Mediators of inflammation*. 2013;2013.
7. Folkman J. Tumor angiogenesis: therapeutic implications. *New england journal of medicine*. 1971;285(21):1182-6.
8. Forsythe JA, Jiang B-H, Iyer NV, Agani F, Leung SW, Koos RD, et al. Activation of vascular endothelial growth factor gene transcription by hypoxia-inducible factor 1. *Molecular and cellular biology*. 1996;16(9):4604-13.
9. Milosevic V, Edelmann RJ, Fosse JH, Östman A, Akslen LA. Molecular Phenotypes of Endothelial Cells in Malignant Tumors. *Biomarkers of the Tumor Microenvironment*: Springer; 2022. p. 31-52.

10. Shibuya M. Vascular endothelial growth factor (VEGF) and its receptor (VEGFR) signaling in angiogenesis: a crucial target for anti-and pro-angiogenic therapies. *Genes & cancer*. 2011;2(12):1097-105.
11. Ahluwalia A, K Jones M, Matysiak-Budnik T, S Tarnawski A. VEGF and colon cancer growth beyond angiogenesis: does VEGF directly mediate colon cancer growth via a non-angiogenic mechanism? *Current Pharmaceutical Design*. 2014;20(7):1041-4.
12. Choueiri TK, Kaelin Jr WG. Targeting the HIF2–VEGF axis in renal cell carcinoma. *Nature medicine*. 2020;26(10):1519-30.
13. Musumeci F, Radi M, Brullo C, Schenone S. Vascular endothelial growth factor (VEGF) receptors: drugs and new inhibitors. *Journal of medicinal chemistry*. 2012;55(24):10797-822.
14. Zhou Y, Zhu X, Cui H, Shi J, Yuan G, Shi S, et al. The role of the VEGF family in coronary heart disease. *Frontiers in cardiovascular medicine*. 2021;8:738325.
15. Stutfeld E, Ballmer- Hofer K. Structure and function of VEGF receptors. *IUBMB life*. 2009;61(9):915-22.
16. Yang X, Cepko CL. Flk-1, a receptor for vascular endothelial growth factor (VEGF), is expressed by retinal progenitor cells. *Journal of Neuroscience*. 1996;16(19):6089-99.
17. Cattaneo F, Castaldo M, Parisi M, Faraonio R, Esposito G, Ammendola R. Formyl peptide receptor 1 modulates endothelial cell functions by NADPH oxidase-dependent VEGFR2 transactivation. *Oxidative medicine and cellular longevity*. 2018;2018.
18. Takahashi T, Yamaguchi S, Chida K, Shibuya M. A single autophosphorylation site on KDR/Flk-1 is essential for VEGF-A-dependent activation of PLC- $\gamma$  and DNA synthesis in vascular endothelial cells. *The EMBO journal*. 2001;20(11):2768-78.
19. Tugues S, Honjo S, König C, Padhan N, Kroon J, Gualandi L, et al. Tetraspanin CD63 promotes vascular endothelial growth factor receptor 2- $\beta$ 1 integrin complex formation, thereby regulating activation and downstream signaling in endothelial cells in vitro and in vivo. *Journal of Biological Chemistry*. 2013;288(26):19060-71.
20. Park SA, Jeong MS, Ha K-T, Jang SB. Structure and function of vascular endothelial growth factor and its receptor system. *BMB reports*. 2018;51(2):73.
21. Attwood MM, Fabbro D, Sokolov AV, Knapp S, Schiöth HB. Trends in kinase drug discovery: Targets, indications and inhibitor design. *Nature Reviews Drug Discovery*. 2021;20(11):839-61.
22. Shang XF, Morris- Natschke SL, Liu YQ, Guo X, Xu XS, Goto M, et al. Biologically active quinoline and quinazoline alkaloids part I. *Medicinal research reviews*. 2018;38(3):775-828.
23. Zayed MF. Medicinal Chemistry of Quinazolines as Analgesic and Anti-Inflammatory Agents. *ChemEngineering*. 2022;6(6):94.
24. Al-Salahi R, Anouar E-H, Marzouk M, Taie HA, Abuelizz HA. Screening and evaluation of antioxidant activity of some 1, 2, 4-triazolo [1, 5-a] quinazoline derivatives. *Future Medicinal Chemistry*. 2018;10(4):379-90.
25. Alafeefy AM, Kadi AA, Al-Deeb OA, El-Tahir KE, Al-Jaber NA. Synthesis, analgesic and anti-inflammatory evaluation of some novel quinazoline derivatives. *European Journal of Medicinal Chemistry*. 2010;45(11):4947-52.
26. Gatadi S, Lakshmi TV, Nanduri S. 4 (3H)-Quinazolinone derivatives: Promising antibacterial drug leads. *European journal of medicinal chemistry*. 2019;170:157-72.

27. Schleiss M, Eickhoff J, Auerochs S, Leis M, Abele S, Rechter S, et al. Protein kinase inhibitors of the quinazoline class exert anti-cytomegaloviral activity in vitro and in vivo. *Antiviral research*. 2008;79(1):49-61.
28. El-Zahabi MA, Elbendary ER, Bamanie FH, Radwan MF, Ghareib SA, Eissa IH. Design, synthesis, molecular modeling and anti-hyperglycemic evaluation of phthalimide-sulfonylurea hybrids as PPAR $\gamma$  and SUR agonists. *Bioorganic chemistry*. 2019;91:103115.
29. Asif M. Chemical characteristics, synthetic methods, and biological potential of quinazoline and quinazolinone derivatives. *International journal of medicinal chemistry*. 2014;2014.
30. Honkanen E, Pippuri A, Kairisalo P, Nore P, Karppanen H, Paakkari I. Synthesis and antihypertensive activity of some new quinazoline derivatives. *Journal of medicinal chemistry*. 1983;26(10):1433-8.
31. Alagarsamy V, Chitra K, Saravanan G, Solomon VR, Sulthana M, Narendhar B. An overview of quinazolines: Pharmacological significance and recent developments. *European journal of medicinal chemistry*. 2018;151:628-85.
32. Faraji A, Motahari R, Hasanvand Z, Bakhshaiesh TO, Toolabi M, Moghimi S, et al. Quinazolin-4 (3H)-one based agents bearing thiadiazole-urea: Synthesis and evaluation of anti-proliferative and antiangiogenic activity. *Bioorganic Chemistry*. 2021;108:104553.
33. Bansal R, Malhotra A. Therapeutic progression of quinazolines as targeted chemotherapeutic agents. *European Journal of Medicinal Chemistry*. 2021;211:113016.
34. Sharma B, Singh VJ, Chawla PA. Epidermal growth factor receptor inhibitors as potential anticancer agents: An update of recent progress. *Bioorganic Chemistry*. 2021;116:105393.
35. Liu X-J, Zhao H-C, Hou S-J, Zhang H-J, Cheng L, Yuan S, et al. Recent development of multi-target VEGFR-2 inhibitors for the cancer therapy. *Bioorganic Chemistry*. 2023:106425.
36. Commander H, Whiteside G, Perry C. Vandetanib: first global approval. *Drugs*. 2011;71(10):1355-65.
37. Shirley M. Fruquintinib: first global approval. *Drugs*. 2018;78:1757-61.
38. Orbegoso C, Marquina G, George A, Banerjee S. The role of Cediranib in ovarian cancer. *Expert Opinion on Pharmacotherapy*. 2017;18(15):1637-48.
39. Modi SJ, Kulkarni VM. Exploration of structural requirements for the inhibition of VEGFR-2 tyrosine kinase: Binding site analysis of type II, 'DFG-out' inhibitors. *Journal of Biomolecular Structure and Dynamics*. 2022;40(12):5712-27.
40. Huang L, Huang Z, Bai Z, Xie R, Sun L, Lin K. Development and strategies of VEGFR-2/KDR inhibitors. *Future Medicinal Chemistry*. 2012;4(14):1839-52.
41. Yousefian M, Ghodsi R. Structure–activity relationship studies of indolin- 2- one derivatives as vascular endothelial growth factor receptor inhibitors and anticancer agents. *Archiv der Pharmazie*. 2020;353(12):2000022.
42. Elkaeed EB, Taghour MS, Mahdy HA, Eldehna WM, El-Deeb NM, Kenawy AM, et al. New quinoline and isatin derivatives as apoptotic VEGFR-2 inhibitors: design, synthesis, anti-proliferative activity, docking, ADMET, toxicity, and MD simulation studies. *Journal of Enzyme Inhibition and Medicinal Chemistry*. 2022;37(1):2191-205.
43. Chen F, Fang Y, Zhao R, Le J, Zhang B, Huang R, et al. Evolution in medicinal chemistry of sorafenib derivatives for hepatocellular carcinoma. *European Journal of Medicinal Chemistry*. 2019;179:916-35.

44. Sun W, Hu S, Fang S, Yan H. Design, synthesis and biological evaluation of pyrimidine-based derivatives as VEGFR-2 tyrosine kinase inhibitors. *Bioorganic Chemistry*. 2018;78:393-405.
45. Roskoski Jr R. Classification of small molecule protein kinase inhibitors based upon the structures of their drug-enzyme complexes. *Pharmacological research*. 2016;103:26-48.
46. Wang B, Wu H, Hu C, Wang H, Liu J, Wang W, et al. An overview of kinase downregulators and recent advances in discovery approaches. *Signal Transduction and Targeted Therapy*. 2021;6(1):423.
47. Hennequin LF, Thomas AP, Johnstone C, Stokes ES, Plé PA, Lohmann J-JM, et al. Design and structure- activity relationship of a new class of potent VEGF receptor tyrosine kinase inhibitors. *Journal of medicinal chemistry*. 1999;42(26):5369-89.
48. Hennequin LF, Stokes ES, Thomas AP, Johnstone C, Plé PA, Ogilvie DJ, et al. Novel 4-anilinoquinazolines with C-7 basic side chains: design and structure activity relationship of a series of potent, orally active, VEGF receptor tyrosine kinase inhibitors. *Journal of medicinal chemistry*. 2002;45(6):1300-12.
49. Newton R, Bowler KA, Burns EM, Chapman PJ, Fairweather EE, Fritzl SJ, et al. The discovery of 2-substituted phenol quinazolines as potent RET kinase inhibitors with improved KDR selectivity. *European Journal of Medicinal Chemistry*. 2016;112:20-32.
50. Bang KC, Song TH, Park YJ, Lee JS, Jun S, Jung SH, et al. Synthesis of 4- anilinoquinazoline- derivative dual kinase inhibitors targeting EGFR and VEGFR- 2. *Bulletin of the Korean Chemical Society*. 2018;39(1):123-5.
51. Ott I, Gust R. Non platinum metal complexes as anti- cancer drugs. *Archiv der Pharmazie: An International Journal Pharmaceutical and Medicinal Chemistry*. 2007;340(3):117-26.
52. De Bock K, Mazzone M, Carmeliet P. Antiangiogenic therapy, hypoxia, and metastasis: risky liaisons, or not? *Nature reviews Clinical oncology*. 2011;8(7):393-404.
53. Wei H, Li D, Yang X, Shang H, Fan S, Li Y, et al. Design and synthesis of vandetanib derivatives containing nitroimidazole groups as tyrosine kinase inhibitors in normoxia and hypoxia. *Molecules*. 2016;21(12):1693.
54. Wei H, Duan Y, Gou W, Cui J, Ning H, Li D, et al. Design, synthesis and biological evaluation of novel 4-anilinoquinazoline derivatives as hypoxia-selective EGFR and VEGFR-2 dual inhibitors. *European Journal of Medicinal Chemistry*. 2019;181:111552.
55. Lee C-I, Liao C-B, Chen C-S, Cheng F-Y, Chung Y-H, Wang Y-C, et al. Design and synthesis of 4-anilinoquinazolines as Raf kinase inhibitors. Part 1. Selective B-Raf/B-RafV600E and potent EGFR/VEGFR2 inhibitory 4-(3-hydroxyanilino)-6-(1H-1, 2, 3-triazol-4-yl) quinazolines. *Bioorganic Chemistry*. 2021;109:104715.
56. Ho TC, Chan AH, Ganesan A. Thirty years of HDAC inhibitors: 2020 insight and hindsight. *Journal of medicinal chemistry*. 2020;63(21):12460-84.
57. Peng F-W, Wu T-T, Ren Z-W, Xue J-Y, Shi L. Hybrids from 4-anilinoquinazoline and hydroxamic acid as dual inhibitors of vascular endothelial growth factor receptor-2 and histone deacetylase. *Bioorganic & Medicinal Chemistry Letters*. 2015;25(22):5137-41.
58. Peng F-W, Xuan J, Wu T-T, Xue J-Y, Ren Z-W, Liu D-K, et al. Design, synthesis and biological evaluation of N-phenylquinazolin-4-amine hybrids as dual inhibitors of VEGFR-2 and HDAC. *European journal of medicinal chemistry*. 2016;109:1-12.

59. Choudhary S, Doshi A, Lockett-Chastain L, Ilnat M, Hamel E, Mooberry SL, et al. Potential of substituted quinazolines to interact with multiple targets in the treatment of cancer. *Bioorganic & medicinal chemistry*. 2021;35:116061.
60. Zhu J-J, Kesari S, Recht L. Phase ii study of verubulin (azixa, mpc-6827) with radiation therapy and temozolomide in newly diagnosed glioblastoma multiforme patients: incomplete report on safety, tolerability and responses (p3. 125). *AAN Enterprises*; 2015.
61. Conconi MT, Marzaro G, Urbani L, Zanusso I, Di Liddo R, Castagliuolo I, et al. Quinazoline-based multi-tyrosine kinase inhibitors: synthesis, modeling, antitumor and antiangiogenic properties. *European journal of medicinal chemistry*. 2013;67:373-83.
62. Xu P, Chu J, Li Y, Wang Y, He Y, Qi C, et al. Novel promising 4-anilinoquinazoline-based derivatives as multi-target RTKs inhibitors: Design, molecular docking, synthesis, and antitumor activities in vitro and vivo. *Bioorganic & Medicinal Chemistry*. 2019;27(20):114938.
63. Li WW, Chen JJ, Zheng RL, Zhang WQ, Cao ZX, Yang LL, et al. Taking Quinazoline as a General Support- Nog to Design Potent and Selective Kinase Inhibitors: Application to FMS- like Tyrosine Kinase 3. *ChemMedChem: Chemistry Enabling Drug Discovery*. 2010;5(4):513-6.
64. Zhang S, Cao Z, Tian H, Shen G, Ma Y, Xie H, et al. SKLB1002, a Novel Potent Inhibitor of VEGF Receptor 2 Signaling, Inhibits Angiogenesis and Tumor Growth In Vivo SKLB1002 Inhibits Angiogenesis and Tumor Growth. *Clinical cancer research*. 2011;17(13):4439-50.
65. Othman EM, Fayed EA, Husseiny EM, Abulkhair HS. The effect of novel synthetic semicarbazone-and thiosemicarbazone-linked 1, 2, 3-triazoles on the apoptotic markers, VEGFR-2, and cell cycle of myeloid leukemia. *Bioorganic Chemistry*. 2022;127:105968.
66. Kubo K, Shimizu T, Ohyama S-i, Murooka H, Iwai A, Nakamura K, et al. Novel potent orally active selective VEGFR-2 tyrosine kinase inhibitors: synthesis, structure– activity relationships, and antitumor activities of n-phenyl-n ‘-{4-(4-quinolyloxy) phenyl} ureas. *Journal of medicinal chemistry*. 2005;48(5):1359-66.
67. Nakamura K, Yamamoto A, Kamishohara M, Takahashi K, Taguchi E, Miura T, et al. KRN633: a selective inhibitor of vascular endothelial growth factor receptor-2 tyrosine kinase that suppresses tumor angiogenesis and growth. *Molecular cancer therapeutics*. 2004;3(12):1639-49.
68. Garofalo A, Goossens L, Lemoine A, Farce A, Arlot Y, Depreux P. Quinazoline-urea, new protein kinase inhibitors in treatment of prostate cancer. *Journal of Enzyme Inhibition and Medicinal Chemistry*. 2010;25(2):158-71.
69. Nozal V, García- Rubia A, Cuevas EP, Pérez C, Tosat- Bitrián C, Bartolomé F, et al. From Kinase Inhibitors to Multitarget Ligands as Powerful Drug Leads for Alzheimer's Disease using Protein- Templated Synthesis. *Angewandte Chemie*. 2021;133(35):19493-503.
70. Garofalo A, Goossens L, Lemoine A, Ravez S, Six P, Howsam M, et al. [4-(6, 7-Disubstituted quinazolin-4-ylamino) phenyl] carbamic acid esters: a novel series of dual EGFR/VEGFR-2 tyrosine kinase inhibitors. *MedChemComm*. 2011;2(1):65-72.
71. Garofalo A, Goossens L, Six P, Lemoine A, Ravez S, Farce A, et al. Impact of aryloxy-linked quinazolines: A novel series of selective VEGFR-2 receptor tyrosine kinase inhibitors. *Bioorganic & medicinal chemistry letters*. 2011;21(7):2106-12.
72. Garofalo A, Farce A, Ravez Sv, Lemoine Al, Six P, Chavatte P, et al. Synthesis and structure–activity relationships of (aryloxy) quinazoline ureas as novel, potent, and selective

- vascular endothelial growth factor receptor-2 inhibitors. *Journal of Medicinal Chemistry*. 2012;55(3):1189-204.
73. Ravez S, Barczyk A, Six P, Cagnon A, Garofalo A, Goossens L, et al. Inhibition of tumor cell growth and angiogenesis by 7-aminoalkoxy-4-aryloxy-quinazoline ureas, a novel series of multi-tyrosine kinase inhibitors. *European Journal of Medicinal Chemistry*. 2014;79:369-81.
74. Ravez S, Arsenlis S, Barczyk A, Dupont A, Frédérick R, Hesse S, et al. Synthesis and biological evaluation of di-aryl urea derivatives as c-Kit inhibitors. *Bioorganic & Medicinal Chemistry*. 2015;23(22):7340-7.
75. Yu B, Li Y-l, Song S-h, Ji X-l, Lin M-s, Wu C-F. Design, synthesis and antitumor activity of 4-aminoquinazoline derivatives targeting VEGFR-2 tyrosine kinase. *Bioorganic & medicinal chemistry letters*. 2012;22(1):110-4.
76. Zhang H-Q, Gong F-H, Ye J-Q, Zhang C, Yue X-H, Li C-G, et al. Design and discovery of 4-anilinoquinazoline-urea derivatives as dual TK inhibitors of EGFR and VEGFR-2. *European Journal of Medicinal Chemistry*. 2017;125:245-54.
77. Qin X, Li Z, Yang L, Liu P, Hu L, Zeng C, et al. Discovery of new [1, 4] dioxino [2, 3-f] quinazoline-based inhibitors of EGFR including the T790M/L858R mutant. *Bioorganic & Medicinal Chemistry*. 2016;24(13):2871-81.
78. Fan H, Wei D, Zheng K, Qin X, Yang L, Yang Y, et al. Discovery of Dioxino [2, 3-f] quinazoline derivative VEGFR-2 inhibitors exerting significant antiproliferative activity in HUVECs and mice. *European Journal of Medicinal Chemistry*. 2019;175:349-56.
79. Abd El Hadi SR, Lasheen DS, Soliman DH, Elrazaz EZ, Abouzid KA. Scaffold hopping and redesign approaches for quinazoline based urea derivatives as potent VEGFR-2 inhibitors. *Bioorganic Chemistry*. 2020;101:103961.
80. Zhang Y, Chen Y, Zhang D, Wang L, Lu T, Jiao Y. Discovery of novel potent VEGFR-2 inhibitors exerting significant antiproliferative activity against cancer cell lines. *Journal of medicinal chemistry*. 2018;61(1):140-57.
81. Elsayed NM, Abou El Ella DA, Serya RA, Tolba MF, Shalaby R, Abouzid KA. Design, synthesis and biological evaluation of indazole-pyrimidine based derivatives as anticancer agents with anti-angiogenic and antiproliferative activities. *MedChemComm*. 2016;7(5):881-99.
82. Elsayed NM, Serya RA, Tolba MF, Ahmed M, Barakat K, Abou El Ella DA, et al. Design, synthesis, biological evaluation and dynamics simulation of indazole derivatives with antiangiogenic and antiproliferative anticancer activity. *Bioorganic Chemistry*. 2019;82:340-59.
83. Potashman MH, Bready J, Coxon A, DeMelfi TM, DiPietro L, Doerr N, et al. Design, synthesis, and evaluation of orally active benzimidazoles and benzoxazoles as vascular endothelial growth factor-2 receptor tyrosine kinase inhibitors. *Journal of medicinal chemistry*. 2007;50(18):4351-73.
84. Shi L, Wu T-T, Wang Z, Xue J-Y, Xu Y-G. Discovery of quinazolin-4-amines bearing benzimidazole fragments as dual inhibitors of c-Met and VEGFR-2. *Bioorganic & Medicinal Chemistry*. 2014;22(17):4735-44.
85. Helfrich BA, Kim J, Gao D, Chan DC, Zhang Z, Tan A-C, et al. Barasertib (AZD1152), a small molecule Aurora B inhibitor, inhibits the growth of SCLC cell lines in vitro and in vivo. *Molecular cancer therapeutics*. 2016;15(10):2314-22.
86. Plé PA, Jung F, Ashton S, Hennequin L, Laine R, Morgentin R, et al. Discovery of AZD2932, a new quinazoline ether inhibitor with high affinity for VEGFR-2 and PDGFR tyrosine kinases. *Bioorganic & medicinal chemistry letters*. 2012;22(1):262-6.

87. Kettle JG, Anjum R, Barry E, Bhavsar D, Brown C, Boyd S, et al. Discovery of N-(4-{{5-Fluoro-7-(2-methoxyethoxy) quinazolin-4-yl} amino} phenyl)-2-[4-(propan-2-yl)-1 H-1, 2, 3-triazol-1-yl] acetamide (AZD3229), a Potent Pan-KIT Mutant Inhibitor for the Treatment of Gastrointestinal Stromal Tumors. *Journal of Medicinal Chemistry*. 2018;61(19):8797-810.
88. Zhang H-Q, Gong F-H, Li C-G, Zhang C, Wang Y-J, Xu Y-G, et al. Design and discovery of 4-anilinoquinazoline-acylamino derivatives as EGFR and VEGFR-2 dual TK inhibitors. *European journal of medicinal chemistry*. 2016;109:371-9.
89. Wang R, Liu H, You Y-Y, Wang X-Y, Lv B-B, Cao L-Q, et al. Discovery of novel VEGFR-2 inhibitors embedding 6, 7-dimethoxyquinazoline and diarylamide fragments. *Bioorganic & Medicinal Chemistry Letters*. 2021;36:127788.
90. Abdallah AE, Mabrouk RR, Al Ward MMS, Eissa SI, Elkaeed EB, Mehany AB, et al. Synthesis, biological evaluation, and molecular docking of new series of antitumor and apoptosis inducers designed as VEGFR-2 inhibitors. *Journal of Enzyme Inhibition and Medicinal Chemistry*. 2022;37(1):573-91.
91. Ashok A, Thanukrishnan K, Bhojya Naik HS, Shaik AG. 6, 7-Dimethoxy-quinazolin-4-yl-amino-thiophene-2-carboxamides as Potent Inhibitors of VEGF Receptors 1 and 2. *Journal of Heterocyclic Chemistry*. 2017;54(2):1065-70.
92. Ashok A, Thanukrishnan K, Bhojya Naik HS, Ghosh S. 6, 7-Dimethoxy-Quinazolin-4-yl-Amino-Nicotinamide Derivatives as Potent Inhibitors of VEGF Receptor II. *Journal of Heterocyclic Chemistry*. 2017;54(3):1723-8.
93. Ashok A, Thanukrishnan K, Naik HSB, Ghosh S. Novel 4-[5-(Substituted-1, 2, 4-oxadiazol-3-yl) phenylamine] Derivatives of 6, 7-Dimethoxy-quinazolines as Potent Inhibitors of VEGF Receptors I and II. *Asian Journal of Chemistry*. 2016;28(10):2122.
94. Weiss MM, Harmange J-C, Polverino AJ, Bauer D, Berry L, Berry V, et al. Evaluation of a series of naphthamides as potent, orally active vascular endothelial growth factor receptor-2 tyrosine kinase inhibitors. *Journal of medicinal chemistry*. 2008;51(6):1668-80.
95. Sun S, Zhang J, Wang N, Kong X, Fu F, Wang H, et al. Design and discovery of quinazoline-and thiourea-containing sorafenib analogs as EGFR and VEGFR-2 dual TK inhibitors. *Molecules*. 2017;23(1):24.
96. Hamdi A, El-Shafey HW, Othman DI, El-Azab AS, AlSaif NA, Alaa A-M. Design, synthesis, antitumor, and VEGFR-2 inhibition activities of novel 4-anilino-2-vinyl-quinazolines: Molecular modeling studies. *Bioorganic Chemistry*. 2022;122:105710.
97. Farouk AK, Allam HA, Rashwan E, George RF, Abbas SE. Design and synthesis of some new 6-bromo-2-(pyridin-3-yl)-4-substituted quinazolines as multi tyrosine kinase inhibitors. *Bioorganic Chemistry*. 2022;128:106099.
98. Wei D, Fan H, Zheng K, Qin X, Yang L, Yang Y, et al. Synthesis and anti-tumor activity of [1, 4] dioxino [2, 3-f] quinazoline derivatives as dual inhibitors of c-Met and VEGFR-2. *Bioorganic Chemistry*. 2019;88:102916.
99. de Castro Barbosa ML, Lima LM, Tesch R, Sant'Anna CMR, Totzke F, Kubbutat MH, et al. Novel 2-chloro-4-anilino-quinazoline derivatives as EGFR and VEGFR-2 dual inhibitors. *European journal of medicinal chemistry*. 2014;71:1-14.
100. Sun J, Li D-D, Li J-R, Fang F, Du Q-R, Qian Y, et al. Design, synthesis, biological evaluation, and molecular modeling study of 4-alkoxyquinazoline derivatives as potential VEGFR2 kinase inhibitors. *Organic & biomolecular chemistry*. 2013;11(44):7676-86.



101. Qiao F, Yin Y, Shen Y-N, Wang S-F, Sha S, Wu X, et al. Synthesis, molecular modeling, and biological evaluation of quinazoline derivatives containing the 1, 3, 4-oxadiazole scaffold as novel inhibitors of VEGFR2. *RSC Advances*. 2015;5(26):19914-23.
102. Yin Y, Sha S, Wang YT, Wu X, Wang SF, Qiao F, et al. Discovery of New 4- Alkoxyquinazoline- Based Derivatives as Potent VEGFR 2 Inhibitors. *Chemical Biology & Drug Design*. 2015;86(5):1323-9.
103. Xi L, Zhang J-Q, Liu Z-C, Zhang J-H, Yan J-F, Jin Y, et al. Novel 5-anilinoquinazoline-8-nitro derivatives as inhibitors of VEGFR-2 tyrosine kinase: synthesis, biological evaluation and molecular docking. *Organic & Biomolecular Chemistry*. 2013;11(26):4367-78.
104. Zhao Y, Liu F, He G, Li K, Zhu C, Yu W, et al. Discovery of arylamide-5-anilinoquinazoline-8-nitro derivatives as VEGFR-2 kinase inhibitors: synthesis, in vitro biological evaluation and molecular docking. *Bioorganic & Medicinal Chemistry Letters*. 2019;29(23):126711.
105. Zhang L, Shan Y, Li C, Sun Y, Su P, Wang J, et al. Discovery of novel anti-angiogenesis agents. Part 6: Multi-targeted RTK inhibitors. *European Journal of Medicinal Chemistry*. 2017;127:275-85.
106. Zhang L, Shan Y, Ji X, Zhu M, Li C, Sun Y, et al. Discovery and evaluation of triple inhibitors of VEGFR-2, TIE-2 and EphB4 as anti-angiogenic and anti-cancer agents. *Oncotarget*. 2017;8(62):104745.
107. Yang Z, Gu J-M, Ma Q-Y, Xue N, Shi X-W, Wang L, et al. Design, synthesis and antitumor activity of aromatic urea-quinazolines. *Future Medicinal Chemistry*. 2019;11(21):2821-30.
108. Patel HM, Bari P, Karpoormath R, Noolvi M, Thapliyal N, Surana S, et al. Design and synthesis of VEGFR-2 tyrosine kinase inhibitors as potential anticancer agents by virtual based screening. *RSC Advances*. 2015;5(70):56724-71.
109. Ghorab MM, Alsaid MS, Soliman AM, Ragab FA. VEGFR-2 inhibitors and apoptosis inducers: synthesis and molecular design of new benzo [g] quinazolin bearing benzenesulfonamide moiety. *Journal of enzyme inhibition and medicinal chemistry*. 2017;32(1):893-907.
110. Soliman AM, Ghorab MM. Exploration of N-alkyl-2-[(4-oxo-3-(4-sulfamoylphenyl)-3,4-dihydroquinazolin-2-yl) thio] acetamide derivatives as anticancer and radiosensitizing agents. *Bioorganic Chemistry*. 2019;88:102956.
111. Mahdy HA, Ibrahim MK, Metwaly AM, Belal A, Mehany AB, El-Gamal KM, et al. Design, synthesis, molecular modeling, in vivo studies and anticancer evaluation of quinazolin-4 (3H)-one derivatives as potential VEGFR-2 inhibitors and apoptosis inducers. *Bioorganic Chemistry*. 2020;94:103422.
112. Eissa IH, El-Helby A-GA, Mahdy HA, Khalifa MM, Elnagar HA, Mehany AB, et al. Discovery of new quinazolin-4 (3H)-ones as VEGFR-2 inhibitors: Design, synthesis, and anti-proliferative evaluation. *Bioorganic Chemistry*. 2020;105:104380.
113. El-Adl K, El-Helby A-GA, Ayyad RR, Mahdy HA, Khalifa MM, Elnagar HA, et al. Design, synthesis, and anti-proliferative evaluation of new quinazolin-4 (3H)-ones as potential VEGFR-2 inhibitors. *Bioorganic & Medicinal Chemistry*. 2021;29:115872.
114. El- Adl K, El- Helby AGA, Sakr H, El- Hddad SS. Design, synthesis, molecular docking, and anticancer evaluations of 1- benzylquinazoline- 2, 4 (1H, 3H)- dione bearing different moieties as VEGFR- 2 inhibitors. *Archiv der Pharmazie*. 2020;353(8):2000068.

115. Zahran SS, Ragab FA, El-Gazzar MG, Soliman AM, Mahmoud WR, Ghorab MM. Antiproliferative, antiangiogenic and apoptotic effect of new hybrids of quinazoline-4 (3H)-ones and sulfachloropyridazine. *European Journal of Medicinal Chemistry*. 2023;245:114912.
116. Ansari AJ, Joshi G, Yadav UP, Maurya AK, Agnihotri VK, Kalra S, et al. Exploration of Pd-catalysed four-component tandem reaction for one-pot assembly of pyrazolo [1, 5-c] quinazolines as potential EGFR inhibitors. *Bioorganic Chemistry*. 2019;93:103314.
117. Ewes WA, Elmorsy MA, El-Messery SM, Nasr MN. Synthesis, biological evaluation and molecular modeling study of [1, 2, 4]-Triazolo [4, 3-c] quinazolines: New class of EGFR-TK inhibitors. *Bioorganic & medicinal chemistry*. 2020;28(7):115373.
118. Azab AE, Alesawy MS, Eldehna WM, Elwan A, Eissa IH. New [1, 2, 4] triazolo [4, 3- c] quinazoline derivatives as vascular endothelial growth factor receptor- 2 inhibitors and apoptosis inducers: Design, synthesis, docking, and antiproliferative evaluation. *Archiv der Pharmazie*. 2022;355(10):2200133.
119. Abdallah AE, Eissa SI, Al Ward MMS, Mabrouk RR, Mehany AB, El-Zahabi MA. Design, synthesis and molecular modeling of new quinazolin-4 (3H)-one based VEGFR-2 kinase inhibitors for potential anticancer evaluation. *Bioorganic Chemistry*. 2021;109:104695.
120. Ahmed MF, Santali EY, Alsantali RI. Design, Synthesis, and Anticancer Activity of New Quinazoline Derivatives as VEGFR-2 Inhibitors and Apoptosis Inducers. *Russian Journal of General Chemistry*. 2022;92(10):2047-57.
121. Eissa IH, Ibrahim MK, Metwaly AM, Belal A, Mehany AB, Abdelhady AA, et al. Design, molecular docking, in vitro, and in vivo studies of new quinazolin-4 (3H)-ones as VEGFR-2 inhibitors with potential activity against hepatocellular carcinoma. *Bioorganic Chemistry*. 2021;107:104532.
122. Abuelizz HA, Marzouk M, Bakheit AH, Awad HM, Soltan MM, Naglah AM, et al. Antiproliferative and antiangiogenic properties of new VEGFR-2-targeting 2-thioxobenzo [g] quinazoline derivatives (in vitro). *Molecules*. 2020;25(24):5944.
123. Wissner A, Floyd MB, Johnson BD, Fraser H, Ingalls C, Nittoli T, et al. 2-(Quinazolin-4-ylamino)-[1, 4] benzoquinones as covalent-binding, irreversible inhibitors of the kinase domain of vascular endothelial growth factor receptor-2. *Journal of medicinal chemistry*. 2005;48(24):7560-81.
124. Wissner A, Fraser HL, Ingalls CL, Dushin RG, Floyd MB, Cheung K, et al. Dual irreversible kinase inhibitors: quinazoline-based inhibitors incorporating two independent reactive centers with each targeting different cysteine residues in the kinase domains of EGFR and VEGFR-2. *Bioorganic & medicinal chemistry*. 2007;15(11):3635-48.
125. Wang X-R, Wang S, Mu H-X, Xu K-Y, Wang X-T, Shi J-T, et al. Discovery of novel VEGFR-2-PROTAC degraders based on the localization of lysine residues via recruiting VHL for the treatment of gastric cancer. *European Journal of Medicinal Chemistry*. 2022;244:114821.
126. Hyun S, Shin D. Small-molecule inhibitors and degraders targeting KRAS-driven cancers. *International Journal of Molecular Sciences*. 2021;22(22):12142.
127. Shao T, Wang J, Chen J-G, Wang X-M, Li H, Li Y-P, et al. Discovery of 2-methoxy-3-phenylsulfonamino-5-(quinazolin-6-yl or quinolin-6-yl) benzamides as novel PI3K inhibitors and anticancer agents by bioisostere. *European Journal of Medicinal Chemistry*. 2014;75:96-105.
128. Hong D, Zhou B, Zhang B, Ren H, Zhu L, Zheng G, et al. Recent advances in the development of EGFR degraders: PROTACs and LYTACs. *European Journal of Medicinal Chemistry*. 2022:114533.

